Available on CMS information server

CMS NOTE 1997/070

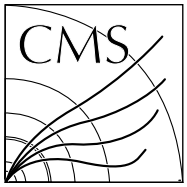

The Compact Muon Solenoid Experiment

CMS Note

Mailing address: CMS CERN, CH-1211 GENEVA 23, Switzerland

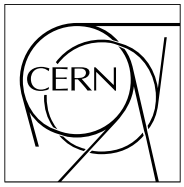

October 20, 1997

On the possibility to observe $h \to b\bar{b}$ with S/B $\sim$ 1 in SUSY (mSUGRA), and implications for tracker and HCAL

S. Abdullin[1], D. Denegri[2]

[1] *ITEP, Moscow, Russia*

[2] *DAPNIA, CEN Saclay, France*

Abstract

We study the possibilities to observe the lightest SUSY scalar Higgs h in the mode $h \to b\bar{b}$ in $\tilde{q}$, $\tilde{g}$ cascade decays in a tagged di-jet effective mass distribution in multijet + E_T^{miss} final states. The idea is to use a strong-interaction production mechanism of $\tilde{q}/\tilde{g}$, exploit the large $h \to b\bar{b}$ branching ratio, and suppress the large $b\bar{b}$ backgrounds with E_T^{miss} and jet cuts. The present investigation is done within the mSUGRA constrained MSSM model. We investigate the influence of the b-tagging efficiency, mistagging probability, geometrical coverage of the CMS microvertex detector and of the hadron calorimeter resolution on the visibility of the peak. Provided the calorimeter system resolution is not significantly worse than $\simeq$ 100 % /$\sqrt{E} \oplus$ 10 % for single hadrons, observation of $h \to b\bar{b}$ is most sensitive to the b-tagging efficiency and and then to the mistagging probability. High b-tagging performance must be assured in the barrel part, up to $\mid \eta^{jet} \mid \simeq 1.5$. We find that there is a very significant part of the mSUGRA parameter space where the $h \to b\bar{b}$ peak can be observed with a signal to background ratio of the order of one. With this model, the lower $\tilde{q}$, $\tilde{g}$ mass limit allowing the detection the h is $\simeq$ 450 GeV, and observation should be possible already with a few $* 10^3$ pb^{-1}, and extends up to $\tilde{q}$, $\tilde{g}$ masses of $\sim$ 1.5 TeV with 10^5 pb^{-1}. The almost entire h mass range from $\simeq$ 80 GeV up to $\simeq$ 125 GeV can be investigated this way. The result should however be valid much more generally provided the $\tilde{q}/\tilde{g} \to \tilde{\chi}_i^0 \to \tilde{\chi}_j^0\ h$ decay chain is kinematically allowed and $\tilde{\chi}_i^0\ \tilde{\chi}_j^0\ h$ coupling is non-vanishing.

1 Introduction

The usual way to search for the lightest CP-even Higgs (h) of the Minimal Super Symmetry Model (MSSM) is through direct Higgs production in gluon fusion or in association with W, $b\bar{b}$ or $t\bar{t}$ and decaying into $\gamma\gamma$, ZZ* $\rightarrow$ 4l, $\mu\mu$ or $b\bar{b}$ [1]. All these production mechanisms are electroweak ones. Each of these channels has however some limitations, such as high tanβ for the $\mu\mu$ mode, or high mass, M$_h$ $\geq$ 130 GeV, and large stop mixing for the ZZ* $\rightarrow$ 4l mode for example. The most general way is nonetheless to search for inclusive $h \rightarrow \gamma\gamma$, which, with 10^5 pb^{-1}, would allow to explore domain approximately given by m$_A$ $\geq$ 250 GeV, tanβ $\geq$ 3 [2]. With the $h \rightarrow \gamma\gamma$ mode we expect a signal on top of a large irreducible $\gamma\gamma$ background with a signal to background ratio of $\leq$ 1/20, as the MSSM Higgs σ_h $*$ branching ratio into the $\gamma\gamma$ mode is always smaller than that of SM Higgs. The instrumental requirements on ECAL are very demanding, a $\gamma\gamma$ effective mass resolution better than 1 GeV at m$_h$ $\simeq$ 100 GeV. In associated production modes $W\ h$, $t\bar{t}\,h$ with $h \rightarrow \gamma\gamma$, the S/B ration is of order of ~ 1 and calorimeter performance is less demanding, but these channels require $\geq 10^5$ pb^{-1} [3]. Evaluations of ways to exploit the $h \rightarrow b\bar{b}$ decay mode in the Wh or $t\bar{t}h$ final states leave only small hope, no ways to have a really significant signal have been found up to now [4].

It is well known that the MSSM h can be abundantly produced in the decays of neutralinos and charginos (primarily $\tilde{\chi}_2^0$). In turn, the $\tilde{\chi}_2^0$ is a typical decay product of squarks and gluinos which are produced abundantly , i.e. with strong interaction cross section. Thus the $h \rightarrow b\bar{b}$ decay can be used for SUSY searches [5]. The idea is to use strongly produced $\tilde{q}$, $\tilde{g}$ and to look for the dominant decay mode $h \rightarrow b\bar{b}$, if $\tilde{\chi}_i^0 \rightarrow h\ \tilde{\chi}_j^0$ is kinematically allowed, and use E$_T^{miss}$ and jet multiplicity cuts to suppress the background.

The large number of SUSY parameters makes it difficult to evaluate the general validity of this approach in the framework of the MSSM, which is just the minimal extension of the Standard Model. So, for an initial investigation we restrict ourselfs at present to the mSUGRA-MSSM model. This model evolves from MSSM, using Grand Unification Theory (GUT) assumptions (see more details in e.g. [6]). It contains only five free parameters :

- a common gaugino mass ($m_{1/2}$)
- a common scalar mass (m_0)
- a common trilinear interaction amongst the scalars (A_0)
- the ratio of the vacuum expectation values of the Higgs fields that couple to $T_3 = 1/2$ and $T_3 = -1/2$ fermions (tanβ)
- a Higgsino mixing parameter sign ($sign(\mu)$)

This much more limited number of parameters allows one more clearly to gauge how fruitful can be this idea. For a given choice of model parameters all the masses, couplings, production cross sections and branching ratios are fixed. At a later stage it can be generalized to the MSSM in which no such constraining mass relations exist.

2 Method

The PYTHIA 5.7 generator [7] is used to generate all SM background processes, whereas ISAJET 7.29 [8] is used for squark and gluino signal simulations. The CMSJET (version 4.3) fast MC package [9] is used to model the CMS detector [1] response; it is coupled with a b-tagging efficiency and mistagging probability obtained from an independent study [10].

The SM background processes considered are : QCD $2 \rightarrow 2$ (including $b\bar{b}$), $t\bar{t}$, Wtb. The $\hat{p}_T$ range of all the background processes is subdivided into several intervals to facilitate accumulation of statistics in the high-$\hat{p}_T$ range : 100-200 GeV (except for QCD), 200-400 GeV, 400-800 GeV and $>$ 800 GeV. The accumulated background statistics for all background channels corresponds to 100 fb^{-1}, except for the QCD jet instrumental mismeasurement background where the statistics corresponds to 0.2 - 50 fb^{-1} depending on the $\hat{p}_T$ interval. It is very difficult to produce a representative sample of QCD jet background in the low-p$_T$ range since the cross section is huge and we need extreme kinematical fluctuations of this type of background to be within the signal selection cuts. So we cannot go confidently below $\simeq$ 150 GeV with the cut on E$_T^{miss}$, where the QCD jet background becomes the dominant contribution and our simulations are not yet fully reliable for this type of background, which depends on the still evolving estimates of dead areas/volumes due to services etc.

Initial requirements for all the samples are the following :

- at least 4 jets with $E_T^{jet} > 20$ GeV in $| \eta^{jet} | < 4.5$
- $E_T^{miss} > 100$ GeV
- Circularity > 0.1

In this analysis in general no specific requirements are put on leptons. If there are isolated muons with $p_T^{\mu} > 10$ GeV within the muon acceptance, or isolated electron with $p_T^e > 10$ GeV within $| \eta^e | < 2.4$ in the event, they are also recorded. The term "isolated lepton" here means satisfying simultaneously the following two requirements :

- no charged particle with $p_T > 2$ GeV in a cone R = 0.3 around the direction of the lepton,
- $\Sigma\ E_T^{cell}$ in a "cone ring" $0.1 < R < 0.3$ around the lepton impact point has to be less than 10 % of the lepton transverse energy

At a later stage we investigate whether selection or vetoing on isolated leptons can possibly help to suppress the SM or other SUSY backgrounds.

3 Signal

In our study we fix only one of the mSUGRA parameters, $A_0 = 0$, and vary the other four : m_0 , $m_{1/2}$, tanβ , sign(μ) . The most pronounced variation of physics quantities (masses, branchings, cross-section) is with m_0 and $m_{1/2}$, thus the investigation is done in the m_0 , $m_{1/2}$ parameter plane for several representative values of tanβ and sign(μ). Since the main source of the lightest Higgses is the decay $\tilde{\chi}_2^0 \to \tilde{\chi}_1^0\ h$, let us fist investigate the domains of parameter space where this decay is allowed. One can see in Figs.1 and 2 that this decay has significant ($\simeq$ 20-90 %) branching ratio in a large portion of parameter space. The lower boundary at $m_{1/2} \sim$ 200-300 GeV corresponds to the three body decays $\tilde{\chi}_2^0 \to \tilde{\chi}_1^0\ q\bar{q}$, $\tilde{\chi}_2^0 \to \tilde{\chi}_1^0\ l^+l^-$ taking over at lower $m_{1/2}$ values where the mass difference $m_{\tilde{\chi}_2^0}$ - $m_{\tilde{\chi}_1^0}$ is not sufficient to allow the $\tilde{\chi}_2^0 \to \tilde{\chi}_1^0\ h$ decay. The boundary at $m_0 \sim$ 200-300 GeV on the other hand corresponds to the opening of two-body cascade modes, e.g. $\tilde{\chi}_2^0 \to \tilde{l}l \to \tilde{\chi}_1^0\ l^+l^-$. Figs.1, 2 also show that the tanβ = 2 , $\mu < 0$ case looks the most promising one, whereas the tanβ = 10, 30, $\mu < 0$ cases seem the worst ones among the possibilities considered, the $\tilde{\chi}_2^0 \to \tilde{\chi}_1^0\ h$ branching ratio being the smallest on average in these cases.

Fig.3 shows total squark and gluino production cross section for the case tanβ = 2 , $\mu < 0$. One can see that total cross-section decreases by $\sim$ 4 orders of magnitude with $m_{1/2}$ increasing from 200 GeV to 800 GeV (in mSUGRA $m_{\tilde{g}} \simeq 2.5\ m_{1/2}$) and also drops by an order of magnitude with m_0 increasing from 200 GeV to 1000 GeV. In contrast, the total cross-section of squark/gluino production varies moderately with tanβ and sign(μ), so a common treatment can be applied similarly for all 6 cases considered in Fig.1 .

Fig.4 shows the parameter space regions excluded either theoretically (dark grey) or experimentally up to now (light grey). LEP II 96/97 data are not included yet. The remaining and largest part of m_0 , $m_{1/2}$ planes is the allowed region. Comparing Fig.4 with 1 and 2, we see that there is a gap between the upper limit explored up to now at $m_{1/2} \simeq$ 100 GeV and the lower limit at $m_{1/2} \simeq$ 200-250 GeV where $\tilde{\chi}_2^0 \to \tilde{\chi}_1^0\ h$ opens up. This comes about as within mSUGRA there are simple mass relations : $M_{\tilde{\chi}_2^0} \simeq 2\ M_{\tilde{\chi}_1^0} \simeq m_{1/2}$, and the LSP mass is typically $\geq$ 100 GeV in the regions where $\tilde{\chi}_2^0 \to \tilde{\chi}_1^0\ h$ is allowed. The range of the h mass varies from $\simeq$ 75 to $\simeq$ 120 GeV, the upper limit is determined by the order to which the radiative corrections have been calculated.

In the framework of mSUGRA with R-parity conservation, sparticles are produced in pairs and the lightest super-particle (LSP) $\tilde{\chi}_1^0$ which appears at the end of each sparticle decay chain produces a significant E_T^{miss}, particularly if the LSP is massive enough. Thus E_T^{miss} provides a powerful rejection tool against backgrounds.

Fig.5 shows an example of production cross sections, masses and decay branching ratios in one typical point in parameter space. This figure is illustrative for the domain of parameter space where $m_{\tilde{g}} > m_{\tilde{q}}$, where gluino decays via squarks and $\simeq$ 1/3 of left squarks decay to $\tilde{\chi}_2^0$ + quark. With increasing m_0 (at fixed $m_{1/2}$) squarks (except of $\tilde{t}_1$) become more massive than gluino at some point (see e.g. Fig.4 in [11]) thus gluino decays into squarks are not more allowed decreasing significantly the yield of $\tilde{\chi}_2^0$ from squark decays. Furthermore, the BR($\tilde{q} \to \tilde{\chi}_2^0\ q$) decreases with increasing m_0 also because the decay $\tilde{q} \to \tilde{g}\ q$ plays an increasingly important role. These various factors, along with the behaviour of the total production cross-section and the variation of the kinematics of the decay chains, make it difficult to predict directly the regions where $h \to b\bar{b}$ could be observed. For a quantative evaluation one needs to investigate the parameter space point by point and optimize cuts accordingly.

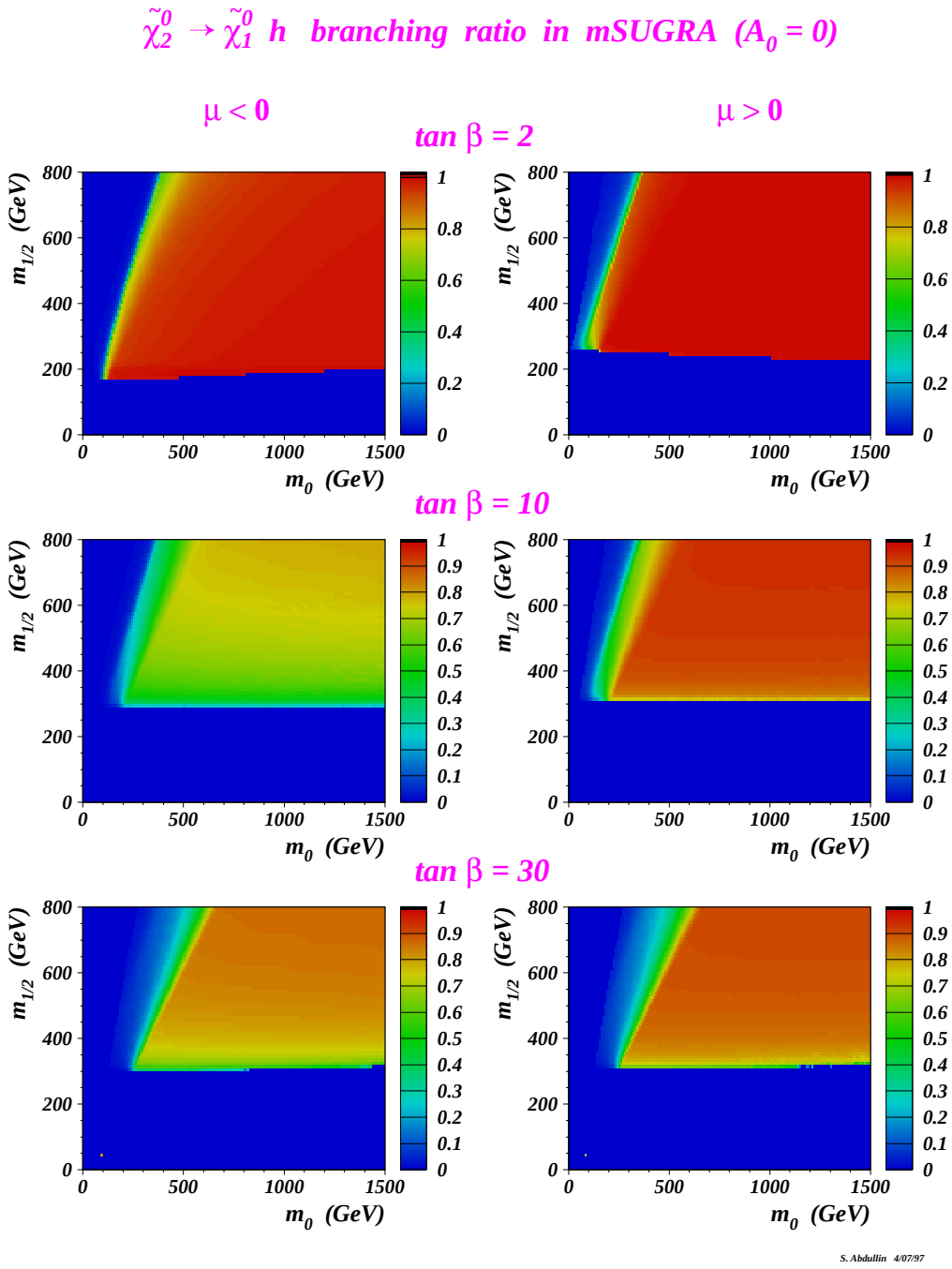

Figure 1: Plots of the $\tilde{\chi}_2^0 \to \tilde{\chi}_1^0\, h$ branching ratio in the m_0, $m_{1/2}$ plane for various parameter values of mSUGRA model.

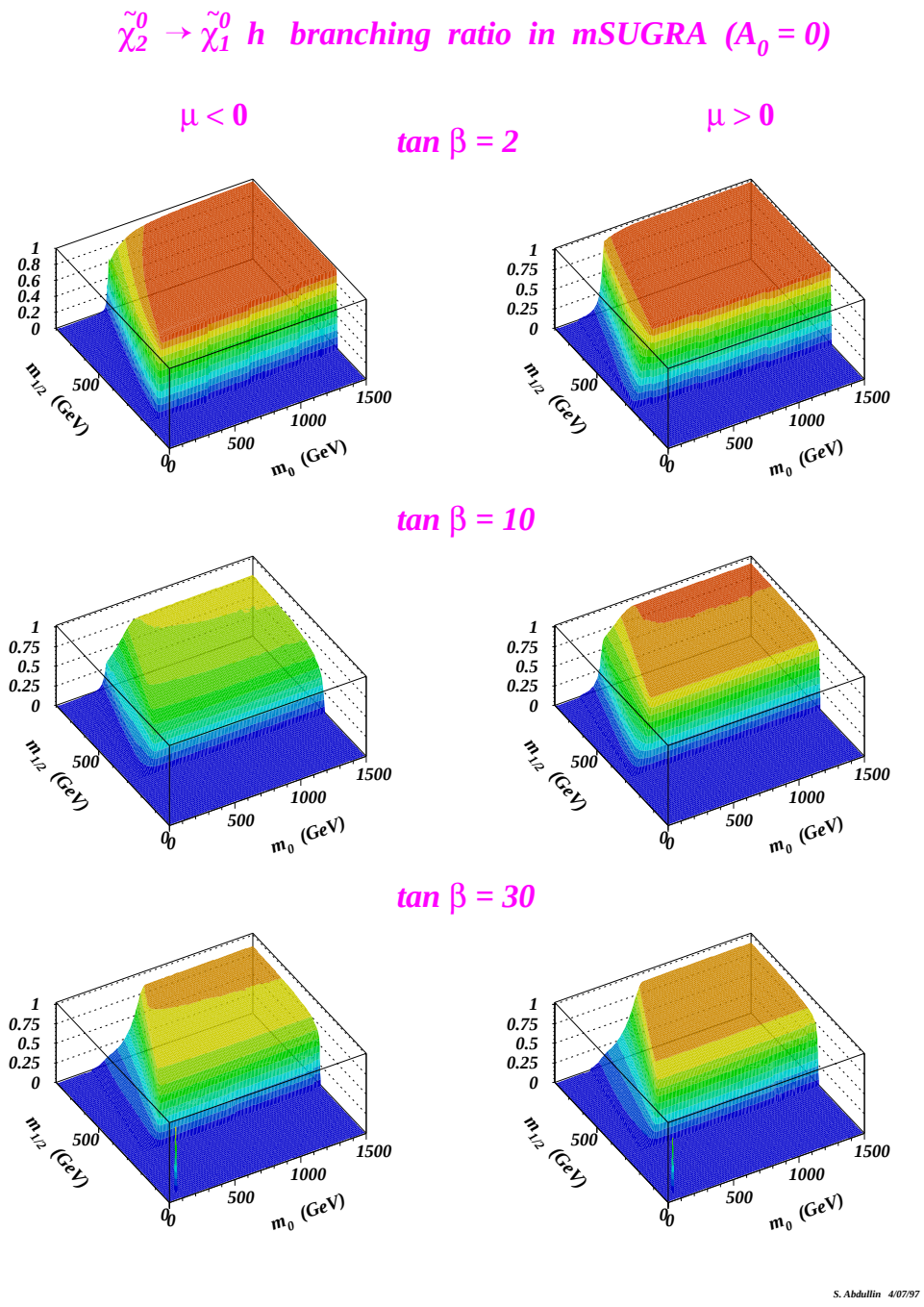

Figure 2: Three-dimensional representation of the $\tilde{\chi}_2^0 \rightarrow \tilde{\chi}_1^0\ h$ branching ratio for different values of mSUGRA model parameters as in Fig.1 .

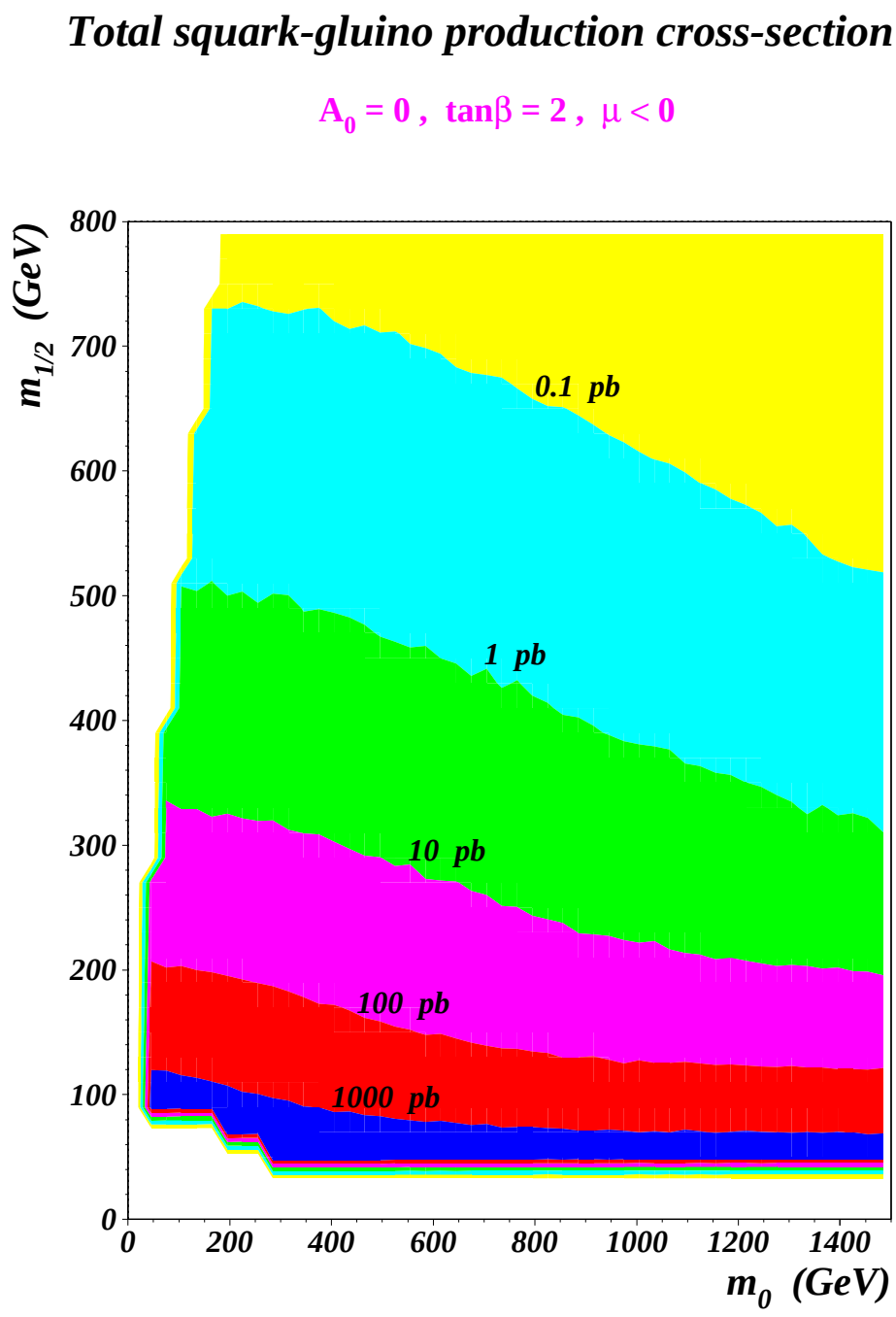

Figure 3: Total squark-gluino cross section as a function of m_0, $m_{1/2}$ for $A_0 = 0$, $\tan\beta = 2$, $\mu < 0$. The empty (white) space in the histogram box denotes part of the parameter space excluded by theory or current experimental data.

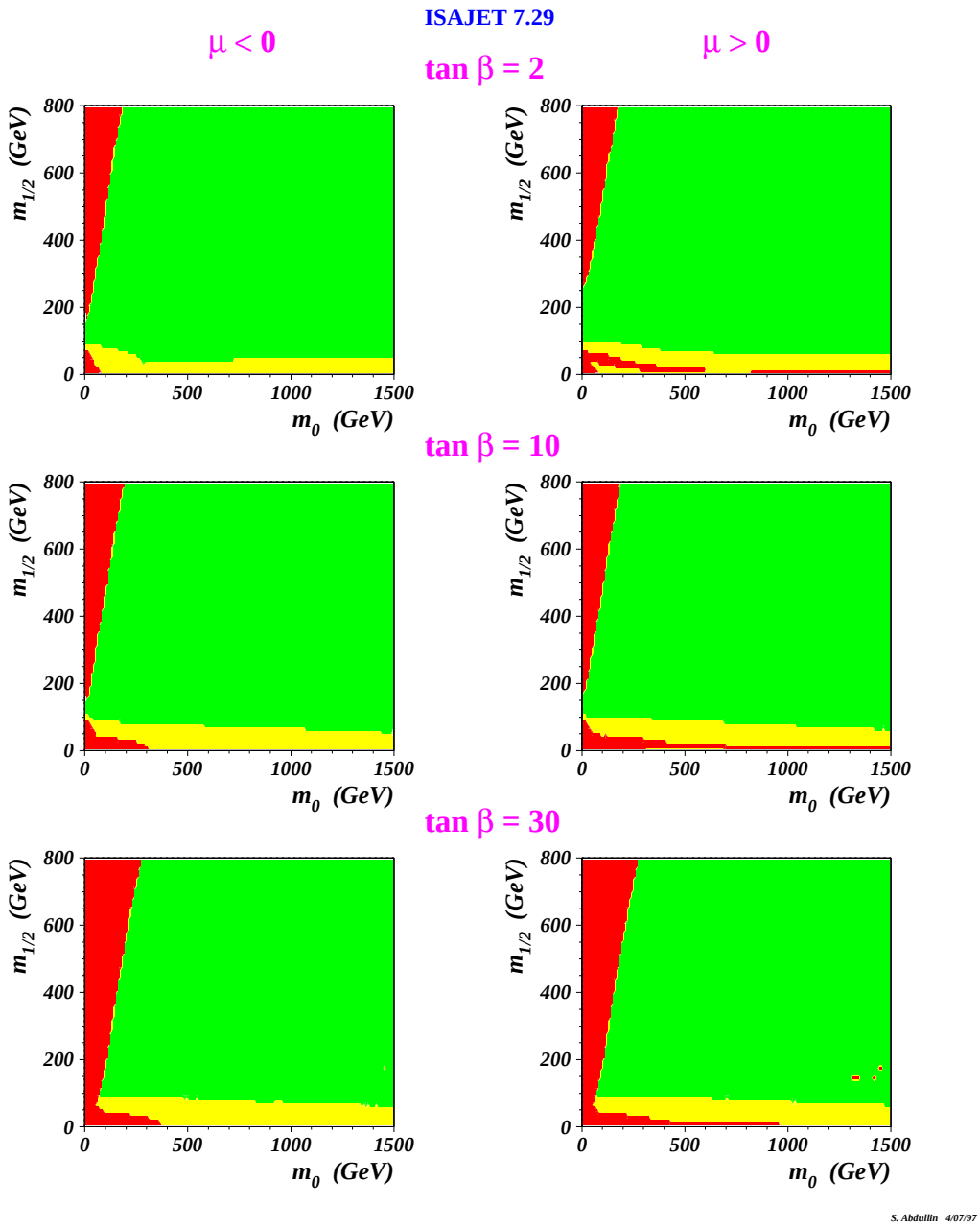

Figure 4: Excluded points of mSUGRA parameter space.

Fig.6 shows the variation of the masses of the relevant sparticles with the sign(μ) and tanβ at a fixed value of m_0 and $m_{1/2}$. The Higgs mass and BR($\tilde{\chi}_2^0 \rightarrow \tilde{\chi}_1^0\ h$) are significantly affected by variations of sign(μ) and tanβ.

Figs.7-8 compare a number of kinematical distributions of the mSUGRA signal with the SM background at two different points in parameter space. These points are rather distant from each other in parameter space, so the kinematics, the"hardness" of the event is significantly different. In both cases it is however evident that the most pronounced difference between signal and background is in the E_T^{miss} distributions. Thus the E_T^{miss} cut is the most important background suppression cut. Of course, the optimal value of this cut depends on the kinematics at the m_0 , $m_{1/2}$ point, as visible from Figs.7 and 8 . A significant difference exists also in the jet multiplicity distributions. Our basic cut is to require at least 4 jets per event, but a specific optimization of cuts on E_T^{miss}, E_T^{jets} etc. is performed in various regions of parameter space.

4 b-tagging with impact parameter

In this study we used the evaluation of the expected b-tagging performance of CMS from impact parameter measurement in the tracker [10]. An example is shown in Fig.9 . The b-tagging probability and mistagging rate for jets is obtained as a function of E_T and jet pseudorapidity. It is obtained from a parameterized gaussian impact parameter resolution dependent on the pixel point resolution, radial position of the pixel layers and the effects of multiple scattering on intervening materials, with the adjunction of a non-gaussian tail based on CDF data. Although there are some specific assumption made concerning the tails of the impact parameter distributions extending beyond the parameterized gaussian parts in [10], the presently on-going study of the expected impact parameter resolution, with full pattern recognition and track finding in CMS [12] is in a good agreement with the results used as an input in the present study.

The b-jet tagging probability is parameterized as a function of E_T in 3 intervals of η : 0 - 1, 1 - 1.75, 1.75 - 2.4 . A typical b-tagging efficiency around $\eta \simeq 0$ for E_T^{jet} = 40 GeV is $\simeq$ 30 %, reaching a maximal efficiency of $\simeq$ 60 % for high-E_T jets in the first η interval. Charm-jets have a typical tagging efficiency (in fact mistagging efficiency !) of about 10 %, and for light quarks and gluons the b-tagging (mistagging) efficiency reaches a maximum of about 3 % for high-E_T jets.

All the jets produced by the event generator are labelled according to their origin. Then, at the analysis stage, they are " b-tagged" according to the b-tagging efficiency or mistagging probability appropriate for quark and gluon types. In our study of $h \rightarrow b\bar{b}$ decays jets are tagged only in the barrel $\mid \eta \mid < 1.75$ interval, if not specially mentioned otherwise.

The tagging efficiency and the purity is expected to be better if one uses b-tagging not only in the transverse plane, but in space, i.e. using also information from the z-coordinates of the pixel detector [13]. This improvement will be implemented later on once the full pattern recognition study is completed, now we assume b-tagging efficiency and purity from measurement in the transverse plane only according to [10]. A further improvement could also include b-tagging with leptons in jets, with however appropriate corrections in jet energy reconstruction.

5 Results

5.1 Low integrated luminosity case, A_0 = 0, tanβ = 2, $\mu < 0$.

Let us consider one point with m_0 = 110 GeV, $m_{1/2}$ = 170 GeV in the lower left corner of the branching ratio plot in Fig.1 . This point corresponds to $m_{\tilde{g}}$ = 466 GeV, $m_{\tilde{u}_L}$ = 422 GeV, $m_{\tilde{\chi}_2^0}$ = 151 GeV, $m_{\tilde{\chi}_1^0}$ = 74 GeV, m_h = 76.5 GeV , it is just beyond the Tevatron reach with $\simeq$ 3 fb^{-1}. The comparison of the signal kinematical distributions at this point with the SM background is shown in Fig.7 . In the *ideal case of 100 % b-tagging efficiency with 0 % mistagging*, one would observe the b-b (jet-jet) mass distribution shown in Fig.10 . In this Figure the initial cuts mentioned above are a little bit hardened, namely $E_T^{miss} > 200$ GeV. From now on, if not specially mentioned otherwise in all di-jet mass distributions we take only one pair of b-jets per event, keeping only jets closest to each other in $\eta - \varphi$ space. No attention is paid to jet "charge" or "leading charge". We remind that no particular treatment is applied to leptons in the analysis, if not stated otherwise.

The "data points" in Fig.10 represent the sum of the mSUGRA $b\bar{b}$-signal and SM and SUSY (combinatorial) backgrounds. The SM background is also shown separately as a shaded histogram. The $b\bar{b}$-mass distribution is fitted with the a sum of a gaussian and a quadratic polynomial. The theoretical prediction of the lightest Higgs mass is indicated with an arrow at the bottom of the plot. The width of the signal peak is determined entirely by

Example of masses and branching ratios at one point in m_0, $m_{1/2}$ space :

- $m_0 = 500$ GeV, $m_{1/2} = 500$ GeV, $A_0 = 0$, $\tan\beta = 2$, $\mu < 0$

$m_{\tilde{g}} = 1224$ GeV $m_{\tilde{q}} \lesssim m_{\tilde{g}}$ $m_{\tilde{t}_1} = 852$ GeV

$m_{\tilde{\chi}_1^0} = 217$ GeV

$m_{\tilde{\chi}_1^\pm} = 427$ GeV $m_{\tilde{e}_L} = 611$ GeV $m_h = 89.7$ GeV

dominant decays :

- $\tilde{g} \rightarrow \tilde{q}\bar{q}$ ($\tilde{t}_1 \bar{t} \sim 49\,\%$, $\tilde{b}_L \bar{b} \sim 17\,\%$)

- $\tilde{q}_L \rightarrow \tilde{\chi}_1^\pm q \sim 2/3$, $\tilde{\chi}_1^0 W^\pm \sim 100\,\%$
  $\tilde{q}_L \rightarrow \tilde{\chi}_2^0 q \sim 1/3$, $\tilde{\chi}_1^0 h \sim 96\,\%$, $b\bar{b} \sim 88\,\%$, $\tilde{\chi}_1^0 Z \sim 3\,\%$

- $\tilde{q}_R \rightarrow \tilde{\chi}_1^0 q \sim 100\,\%$

- $\tilde{t}_1 \rightarrow \tilde{\chi}_1^0 t \sim 94\,\%$, $W^+ b$

event topology :

- *4 b-jets*
  + 3 non-b jets
  + E_t^{miss}

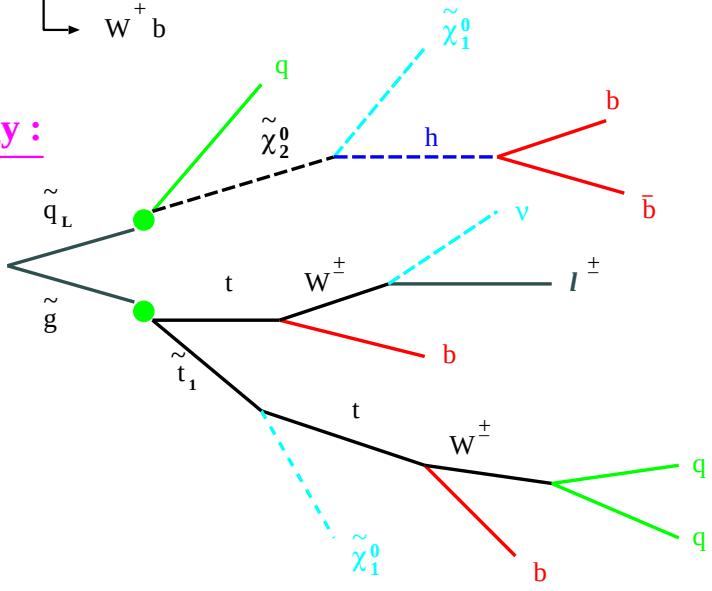

S. Abdullin

Figure 5: Typical signal topology and branching ratios.

Example of masses and branching ratios at some points

● $m_0 = 500$ GeV, $m_{1/2} = 500$ GeV, $A_0 = 0$

tan β / sign (μ)	Masses of sparticles (GeV)						Branchings (%)	
	h	$\tilde{\chi}_1^0$	$\tilde{\chi}_2^0$	$\tilde{g}$	u_L	$\tilde{t}_1$	$\tilde{\chi}_2^0 \to \tilde{\chi}_1^0$ h	h → $\bar{b}$b
2 -	89.7	217.0	426.8	1223.5	1170.3	851.6	95.6	88.2
2 +	99.5	213.0	413.0	1239.6	1180.7	814.9	99.4	87.4
10 -	117.5	214.2	415.3	1234.5	1183.9	891.9	70.2	81.0
10 +	118.7	212.8	409.2	1234.5	1184.0	884.4	92.4	80.0
30 -	119.1	213.7	412.3	1242.7	1183.6	889.1	82.1	80.6
30 +	119.4	213.2	410.2	1242.7	1183.6	886.4	88.5	79.3

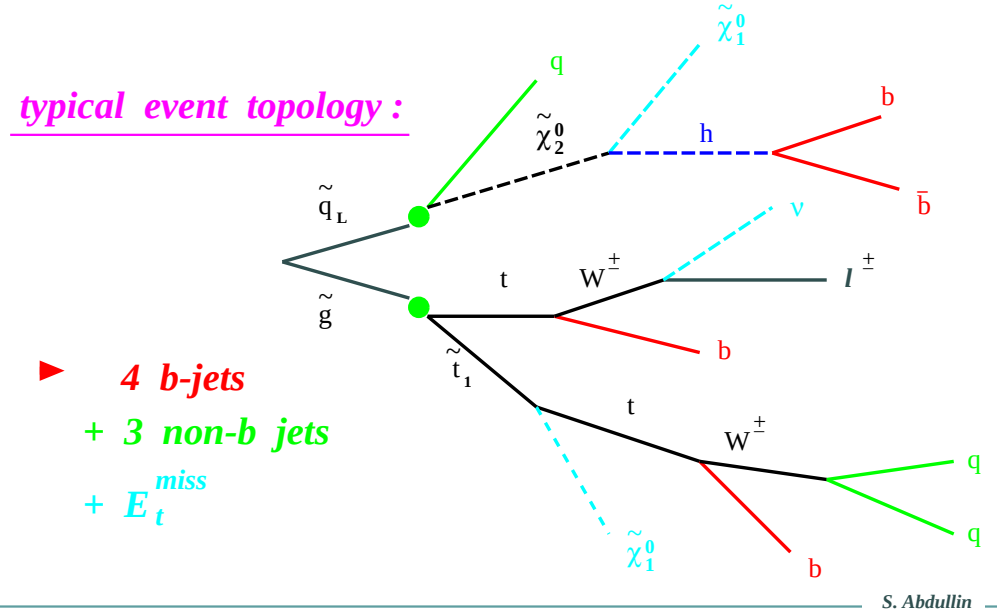

Figure 6: Dependence on tanβ and sign(μ) of particle masses and branching ratios at fixed m_0=$m_{1/2}$=500 GeV.

the jet resolution of the detector, since the intrinsic $h \to b\bar{b}$ decay width varies from 3.2 to 4.3 MeV over the entire mSUGRA parameter space shown in Fig.1 . The position of the peak is shifted to lower mass since energy losses in jets (finite cone size, various thresholds etc.) and typical missing energy for b-jets (caused by neutrinos) are not corrected for.

The three distributions in the lower half in Fig.10 are for events in the M_{bb} mass window 55 - 85 GeV to illustrate the kinematics of the $h \to b\bar{b}$ decay at this particular point with the lowest possible masses of squarks and gluinos (see also Fig.7) where the $\tilde{\chi}_2^0$ still decays into Higgs. The average b-jet transverse energy is $\simeq$ 80 GeV, the b-jets are very central as they result from decay of massive ($\sim$ 500 GeV) squarks and gluinos which are centrally produced. Clearly b-tagging beyond $\mid \eta^{jet} \mid \simeq 1.5$ is not very effective in this search.

The M_{bb} distribution in this particular point, if one applies the "nominal" b-tagging performance expectations described in the previous section, is given in Fig.11 . The lower distribution (with corresponding SM background in dark) is obtained with $E_T^{miss} > 200$ GeV and $E_T^{jet} > 40$ GeV , whilst the upper one (SM is light shaded) corresponds to softer cuts : $E_T^{miss} > 150$ GeV, $E_T^{b-jet} > 20$ GeV in $\mid \eta \mid < 1.75$, $E_T^{non-b-jet} > 40$ GeV in $\mid \eta \mid < 4.5$. In both distributions the "left shoulder" is significantly suppressed when compared to that in Fig.10 , since the tagging efficiency falls quickly with decreasing jet E_T, Fig.9 , thus suppressing events at low M_{bb}. This reduction also causes some sharpening of the peak. Relaxation of the cuts slightly improves the significance, which is calculated as $S/\sqrt{B}$ within a $\pm$ 1σ interval around the peak centre, but the S/B ratio decreases. The SM background is small compared to the mSUGRA signal and SUSY background. The signal peak sits on top of an intrinsic background originating mainly from additional real b-jets in the event (see example in Fig.5), rather than from mistagged jets. An improvement could possibly be obtained taking into account "jet charge" and thus enriching the sample in $b\bar{b}$ pairs as compared to $b\bar{b}$ + bb ($\bar{b}\bar{b}$). This however requires determination of the charges of fast tracks in jets, a task still under study in CMS [12].

It is worth emphasizing that at this point of parameter space the $h \to b\bar{b}$ mass peak is visible already with $\simeq$ 1 fb^{-1} which can be accumulated in $\sim$ a month of LHC running. This is $\leq$ 1/10 of the luminosity needed for observation of $h \to \gamma\gamma$ at this m_0, $m_{1/2}$ point corresponding to $\tilde{g}$, $\tilde{q}$ masses just beyond the Tevatron reach. With an increased integrated luminosity of 2-3 fb^{-1} the part of the m_0, $m_{1/2}$ plane which can be explored is represented by a few points in Fig.12 . All the distributions in this figure are obtained with similar cuts : $E_T^{miss} > 200$ GeV and $E_T^{jet} >$ 40 GeV. The systematic investigation of parameter space reach is given later on.

5.2 Dependence of $h \to b\bar{b}$ observability on detector performance

To investigate instrumental requirements allowing to discover $h \to b\bar{b}$ we choose a point not on the edge of the region of observability, but rather more representative point in parameter space at some distance from the region discussed in a previous subsection, which has harder signal kinematical distributions as visible comparing Fig.7 and 8. The b-jet related distributions for point $m_0 = m_{1/2} = 500$ GeV , $A_0 = 0$, tanβ = 2, $\mu < 0$ in Fig.13 can be compared with analogous ones in Fig.10 for m_0 = 110 GeV, $m_{1/2}$ = 170 GeV .

The distributions in Fig.13 are obtained with harder cuts than those in Fig.10 , namely $E_T^{miss} > 400$ GeV and $E_T^{jet} > 40$ GeV, and correspond to an ideal b-tagging performance, as in Fig.10 .

Figs.14-16 illustrate the sensitivity in the expected $h \to b\bar{b}$ signal induced by various instrumental factors. The distribution in Fig.14a is the "benchmark", since it is obtained with "nominal" performance and selection parameters :

- $E_T^{miss} > 400$ GeV,
- $\geq$ 4 jets with $E_T^{jet} > 40$ GeV,
- b-tagging in $\mid \eta \mid < 1.75$, with nominal b-tagging efficiency and mistagging probability from [10],
- only one pair of b-tagged jets (closest in η, φ space) is chosen from all possible jet-jet combinations.

Under this nominal conditions, with 100 fb^{-1}, the expected signal significance $S/sqrtB$ should be 18.3, Fig.14a . In Fig.14b one can see that if all bb-combinations per event are included in the distribution, the signal to background ratio degrades with signal significance decreasing by $\simeq$ 12 % . Figs.14c and 14d show the effect of increasing, or decreasing, the b-tagging efficiency by 15 % in absolute value, whilst keeping mistagging at the "nominal" level. This means that, if nominally the tagging efficiency is $\sim$ 50 % for E_T^{jet} = 80 GeV in the central region $\mid \eta \mid <$

1.0, Fig.9 , it is changed correspondingly to 65 % or 35 %. The dependence on the b-tagging efficiency is very pronounced, the signal significance varying by respectively $\pm$ 25 % . This is not surprising as b-tagging efficiency enters quadratically in the number of signal events. Figures 15a and 15b illustrate the effect on the observability of the peak of the η acceptance of the silicon pixel detector. As can be expected on basis of Fig.13, increased acceptance beyond $\mid \eta^{jet} \mid \simeq 1.5$ does not bring a significant improvement as these b-jets are very central. With b-tagging acceptance increasing from $\mid \eta^{jet} \mid$ = 1.0 to 1.75 and 2.4, signal significance improves from 17.2 to 18.3 and 18.8 Figures 15c and 15d illustrate the signal dependence on tagging purity, where one keeps the "nominal" b-tagging efficiency, but varies the mistagging rate for all non-b jets, including c-ones. Increasing the mistagging probability by a factor of 3 degrades visibly S/B and signal significance by $\simeq$ 25 % which is rather significant.

Since the observed width of the $h \rightarrow b\bar{b}$ peak is entirely determined by the calorimetric jet-jet effective mass resolution, one can expect some dependence of the signal observability on the energy resolution, as illustrated in Fig.16 . The upper plot is for the nominal HCAL performance, corresponding to σ_E/E = 82 % /$\sqrt{E} \oplus$ 6.5 % at η = 0. The lower plot corresponds to the HCAL energy resolution deteriorated to 120 % /$\sqrt{E} \oplus$ 10 %. To have an impression of the difference in the assumed energy resolution between upper and lower figures, one can compare the resolution on for a single 10 GeV pion : 25 % versus 39 % . The sigma of a gaussian fit to the $\simeq$ 90 GeV Higgs peak is 7.6 GeV in first case and 11 GeV in second one. The difference in S/B between Figs. 16a and b is significant, but not dramatic. This is due to the fact that the $h \rightarrow b\bar{b}$ pair has a significant boost, $p_T^{b\bar{b}}$ $\sim$ 200 GeV in Fig.13 , and the jet-jet opening angle, whose measurement precision is determined by calorimeter granularity plays an important role in the effective mass resolution. It is clear however that we should not allow a jet energy resolution worse than 15 % for an $E_T^{jet} \simeq$ 100 GeV - which corresponds to Fig.16b - without significance performance loss.

Fig.17 illustrates the importance of the tagging efficiency at a point near the limit of the domain where the $h \rightarrow b\bar{b}$ peak can be observed and where the SUSY signal and backgrounds are comparable to the SM background. The "nominal" parameters are the same as mentioned above for Fig.14 . The $\pm$ 15% variation in absolute value of the assumed tagging efficiency induces a corresponding $\pm$ 30 % variation in signal significance. One also can see in this Figure that the additional requirement of absence of an isolated lepton(s) in the event helps to suppress the SM background by a factor of $\sim$ 2 (Fig.17c), although it does not improve much the signal significance. Fig.17d shows that the "visibility" of the signal can be somewhat subjective, the $h \rightarrow b\bar{b}$ peak is barely visible, whilst the calculated significance is rather good nevertheless.

Fig.18 illustrates the $h \rightarrow b\bar{b}$ signal observability as a function of m_h over the allowed range of 80 to 120 GeV. For this we select the points shown in Fig.6 , all at same $m_0 = m_{1/2}$ = 500 GeV, but different values of tanβ and μ , with nominal b-tagging performance and 100 fb^{-1}. One can clearly see that the signal peak becomes broader with increasing Higgs mass since the jet $E_T > 40$ GeV cut-off does not play such a role as for a low-mass peak.

5.3 W $\rightarrow jj$ and Z $\rightarrow b\bar{b}$ decays

It is obvious that W $\rightarrow$ jj decays in $\tilde{g}/\tilde{q}$ cascades can yield a jet-jet signal several times larger than $h \rightarrow b\bar{b}$. A question thus arises what happens if the Higgs mass is close to the W one. Fig.19 serves as an illustration that a signal peak observed in the vicinity of W $\rightarrow$ jj should not be a remnant of a mistagged W peak provided the mistagging probability is as expected in Fig.9 . The parameter space point shown in this Figure is chosen to maximize the mass difference between W and h not to confuse effect of mistagging with mass coincidence. One can see that with nominal b-tagging performance, including mistagging, the W peak is entirely suppressed and only the Higgs peak remains. Fig.19c is the same as Fig.18d. What happens if the mistagging probability is much increased is still under study.

If $\tilde{\chi}_2^0$ is heavy enough to decay into $\tilde{\chi}_1^0$ + Z , this channel competes with $\tilde{\chi}_2^0 \rightarrow \tilde{\chi}_1^0\ h$ thus decreasing the yield of Higgses, especially for high tanβ and negative μ (see Fig.6). Since for all the cases considered in Fig.1 (except the case tanβ = 2 , $\mu < 0$) the Higgs is heavier than the Z, in the lower part of the plots there is a band $\simeq$ parallel to the m_0 axis, just beneath the region under study, where the $\tilde{\chi}_2^0$ decays almost entirely ($>$ 95 %) into Z + $\tilde{\chi}_1^0$, as the $\tilde{\chi}_2^0 \rightarrow \tilde{\chi}_1^0\ h$ is not yet open. The branching ratio of Z $\rightarrow b\bar{b}$ is $\simeq$ 17 %, so, at least in principle , one could observe a Z peak in the tagged di-jet mass distribution (except the case tanβ = 2 , $\mu < 0$), as shown in Fig.20 for the point with m_0 = 200 GeV , $m_{1/2}$ = 250 GeV , A_0 = 0 , tanβ = 10 , $\mu < 0$, where the BR($\tilde{\chi}_2^0 \rightarrow \tilde{\chi}_1^0\ Z$) = 97.6 %. The distributions are obtained with the cuts as appropriate for low luminosity searches : $E_T^{miss} > 200$ GeV and $E_T^{jet} > 40$ GeV. In the major part of parameter space BR ($\tilde{\chi}_2^0 \rightarrow$ Z + $c\tilde{h}i_1^0$) $\ll$ BR ($\tilde{\chi}_2^0 \rightarrow \tilde{\chi}_1^0\ h$) , except for a small marginal region (band) with low BR ($\tilde{\chi}_2^0 \rightarrow \tilde{\chi}_1^0\ h$), for example, in point m_0 = 200 GeV , $m_{1/2}$ = 300 GeV , A_0 = 0 , tanβ = 10, $\mu < 0$ (see Fig.1). So, if a $b\bar{b}$ peak is observed at $\simeq$ 90 GeV and there is an ambiguity as to what is

seen, we shall look at data samples with all cuts and selections kept, except for a b-b pair replaced by $\mu^+\mu^-$ and e^+e^-. In case of Z production, Z $\rightarrow e^+e^-$, $\mu^+\mu^-$ decays should be seen with perfectly calculable rates relative to $b\bar{b}$, whilst no signal should be seen if the $b\bar{b}$ signal is due to h which has negligible branching to electrons and muons. In case that $b\bar{b}/\mu^+\mu^-/e^+e^-$ relative rates are not as expected for pure Z decays, we may have coexistence of both $\tilde{\chi}_2^0$ decay modes, as possible in some points of parameter space. So leptonic decays of the Z can provide information on the fraction of $\tilde{\chi}_2^0 \rightarrow$ Z + $\tilde{\chi}_1^0$ decays and its contribution to the $b\bar{b}$ signal.

5.4 Domains of visibility of $h \rightarrow b\bar{b}$

Now, after discussion of the instrumental requirements allowing observation of $h \rightarrow b\bar{b}$ peak, let us turn to the main problem : how general is the possibility to observe this $h \rightarrow b\bar{b}$ signal in $\tilde{q}$, $\tilde{g}$ decays ?

Fig.21 shows the domain of parameter space where the $h \rightarrow b\bar{b}$ signal is visible with $S/\sqrt{B} > 5$ for the case A_0 = 0, tanβ = 2 , $\mu < 0$ and with "nominal" b-tagging performance of CMS for 10 and 100 fb^{-1}. The outer borders are somewhat approximate, as the question of signal observability depends on the chosen convention whether something is really visible or not (e.g. Fig.17d), even with satisfied quantative criterion, as for example : $S/\sqrt{B} > 5$ or $S/\sqrt{S+B} > 5$. The isomass curves for the lightest CP-even Higgs (h) and CP-odd one (A) are also shown in Fig.21 by dash-dotted lines. The bold broken line denotes the region where BR($\tilde{\chi}_2^0 \rightarrow \tilde{\chi}_1^0\ h$) = 50 %. Some decay modes, characteristic of particular regions of parameter space , as $\tilde{\chi}_2^0 \rightarrow l\hat{l}$, $\tilde{\chi}_2^0 \rightarrow \tilde{\chi}_1^0\ b\bar{b}$ non-resonant etc. are also shown.

The shaded regions along the axes denote the present theoretically ("TH") or experimentally ("EX") excluded regions of parameter space not including yet LEP 96/97 results. The case in Fig.21 , with A_0 = 0, tanβ = 2 , $\mu < 0$ looks like the most promising one among the cases shown in Fig.1 . The threshold of visibility of $h \rightarrow b\bar{b}$ at lowest $m_{1/2}$ = 170-180 GeV, starting at $\leq$ 1 fb^{-1}, corresponds to $m_{\tilde{g},\tilde{q}} \geq$ 400 - 450 GeV, i.e. begins just where Tevatron squark and gluino searches will stop with $\sim$ 5 fb^{-1}. The least favourable case in Fig.1 corresponds to tanβ = 10 , $\mu < 0$. Fig.22 shows the results concerning the domains of the signal visibility for this latter case. In this case there seems to be a significant observability gap and this has to be studied in more details in the future. In Fig.23 one can see the results for some "intemediate" case between best and worst ones in Figs.21 and 22, for tanβ = 30 , $\mu > 0$.

6 Conclusions and future prospects

The search for the $h \rightarrow b\bar{b}$ decay, when the lightest Higgs h is produced in the cascade decays of the strongly interacting sparticles seems to be a promising one. The large rejection factor needed to suppress backgrounds and achieve a S/B of $\sim$ 1 is here provided by the E_T^{miss} cuts. Nothing similar can be obtained in the search for the SM Higgs in H $\rightarrow b\bar{b}$. This way of searching for the h might allow to discover the SUSY Higgs already at a the modest integrated luminosity of few fb^{-1}. The squarks and gluinos must however have a minimal mass in the $\simeq$ 450 to 700 GeV range for this search to be possible in this model. The study carried out here in the mSUGRA framework shows that there is a significant domain of parameter space, just beyond the $\tilde{q}$, $\tilde{q}$ mass reach of the Tevatron ($\sim$ 400-450 GeV), where observation of the $h \rightarrow b\bar{b}$ decay would be possible, assuming a reasonable b-tagging efficiency, already with an integrated luminosity of 1-3 fb^{-1}. The parameter space domain can be significantly extended with 100 fb^{-1}, where $\tilde{g}$, $\tilde{q}$ with masses in 1.5 TeV range are probed. The entire h mass range from $\simeq$ 80 GeV up to $\simeq$ 125 GeV can be covered.

Our investigations show that the observation of the $h \rightarrow b\bar{b}$ signal depends most critically on the b-tagging efficiency and less critically on the mistagging probability ; the acceptance of the b-tagging pixel devices is not critical, provided the coverage is not smaller than $|\ \eta\ | \simeq 1.5$. A calorimetric system resolution of $\simeq 100\ \%/\sqrt{E} \oplus 10\ \%$ is adequate for this type of search, but should not be significantly worse. A significant improvement in b-tagging efficiency could be obtained with a third pixel layer, or having pixel layer at the radius of 4 cm even for high luminosity running, to be replaced every (few) year(s). We remind that whilst efficient b-tagging strongly militates in favour of a pixel layer at 4 cm, the heavy ion physics programme of CMS demands two layers, the inner at 7 cm. The mistagging probability depends on the non-gaussian part of the impact parameter measurement distribution, thus on the overall pattern recognition performance in the region close to the beam i.e. on the balance between Si and MSGC layers in the tracker. This aspect would presumably imply increasing Si layers from 4 to 5, possibly 6, reducing correspondingly MSGC layers and deserves a dedicated study.

Two more aspects should be further studied in the future. From the detector performance point of view a more detailed study should be made on how critical is the overall ECAL + HCAL calorimetric performance in terms of

jet reconstruction for $E_T^{jet} \sim$ 100-200 GeV. A further problem is how useful is in the present case b-tagging with leptons, and what is the effect on the jet-jet mass resolution and peak shift of the escaping neutrinos Furthermore the best balance between pixels, Si and MSGC layers should also be studied in terms of best b-tagging performance.

Second, and most important if this method has to become a viable alternative to the $h \to \gamma\gamma$ search, is to evaluate how general are the results of the present study, i.e. what happens out of the mSUGRA scheme where masses are not so constrained, for example in MSSM. Presumably what is found here in the framework of mSUGRA-MSSM is much more generally valid, i.e. that, as soon as the $\tilde{g}/\tilde{q} \to \tilde{\chi}_2^0 \to \tilde{\chi}_1^0\ h$, or even more generally, the $\tilde{g}/\tilde{q} \to \tilde{\chi}_i^0 \to \tilde{\chi}_j^0\ h$ chain s are kinematically allowed and the $\tilde{\chi}_i^0\ \tilde{\chi}_j^0\ h$ couplings not vanishing, this $h \to b\bar{b}$ search might applicable.

A particular point of interest in this respect is the gap at the lower $\tilde{q}$, $\tilde{g}$ masses, between the domains where SUSY can be explored at the Tevatron with 5-6 fb^{-1} and the lower mass reach of this channel, if it exists in mSUGRA, can it be overcome in MSSM, where mass relations are less rigid ?

References

[1] CMS collaboration, *Technical Proposal*, CERN/LHCC 94-38.

[2] R. Kinnunen, D .Denegri, CMS Note/1997-057.

[3] S. Abdullin, A. Starodumov, N. Stepanov, CMS TN/93-087;
Z. Antunovich, D. Denegri, M. Dzelalija, R. Kinnunen, CMS TN/96-091.

[4] D. Drollinger, T. Muller, R. Kinnunen, presentation at CMS WEEK Physics meeting, June,27, 1997, CMS Note in preparation;
D. Fraidevaux, E. Richter-Was, ATLAS Internal note Phys-NO-043 (1994).

[5] L.Didenko and B.Lund-Jensen, ATLAS Internal Note PHYS-No-42;
I.Hinchliffe et al., Phys.Rev.**D55**(1997) 5520.

[6] H. Baer, C-H. Chen, R. Munroe, F. Paige and X. Tata, Phys.Rev. **D51**(1995)1046.

[7] T. Sjöstrand, *Computer Physics Commun.* 39 (1986) 347; T. Sjöstrand and M. Bengtsson, *Computer Physics Commun.* 43 (1987) 367; H.U. Bengtsson and T. Sjöstrand, *Computer Physics Commun.* 46 (1987) 43; T. Sjöstrand, CERN-TH.7112/93.

[8] F. Paige and S. Protopopescu, in *Supercollider Physics*, p. 41, ed. D. Soper (World Scientific, 1986); H. Baer, F. Paige, S. Protopopescu and X. Tata, in *Proceedings of the Workshop on Physics at Current Accelerators and Superolliders*, ed. J. Hewett, A. White and D. Zeppenfeld (Argonne National Laboratory, 1993).

[9] S. Abdullin, A. Khanov and N. Stepanov, CMS TN/94-180
(see also /afs/cern.ch/user/a/abdullin/public/cmsjet/4.3/cmsjet43.ps).

[10] D. Denegri, R. Kinnunen, CMS TN/96-045.

[11] S. Abdullin, CMS TN/96-095.

[12] A. Khanov, talk given at CMS WEEK Physics meeting, June, 27, 1997;
A. Khanov, N. Stepanov, CMS Note in preparation.

[13] R.Horisberger, private communication.

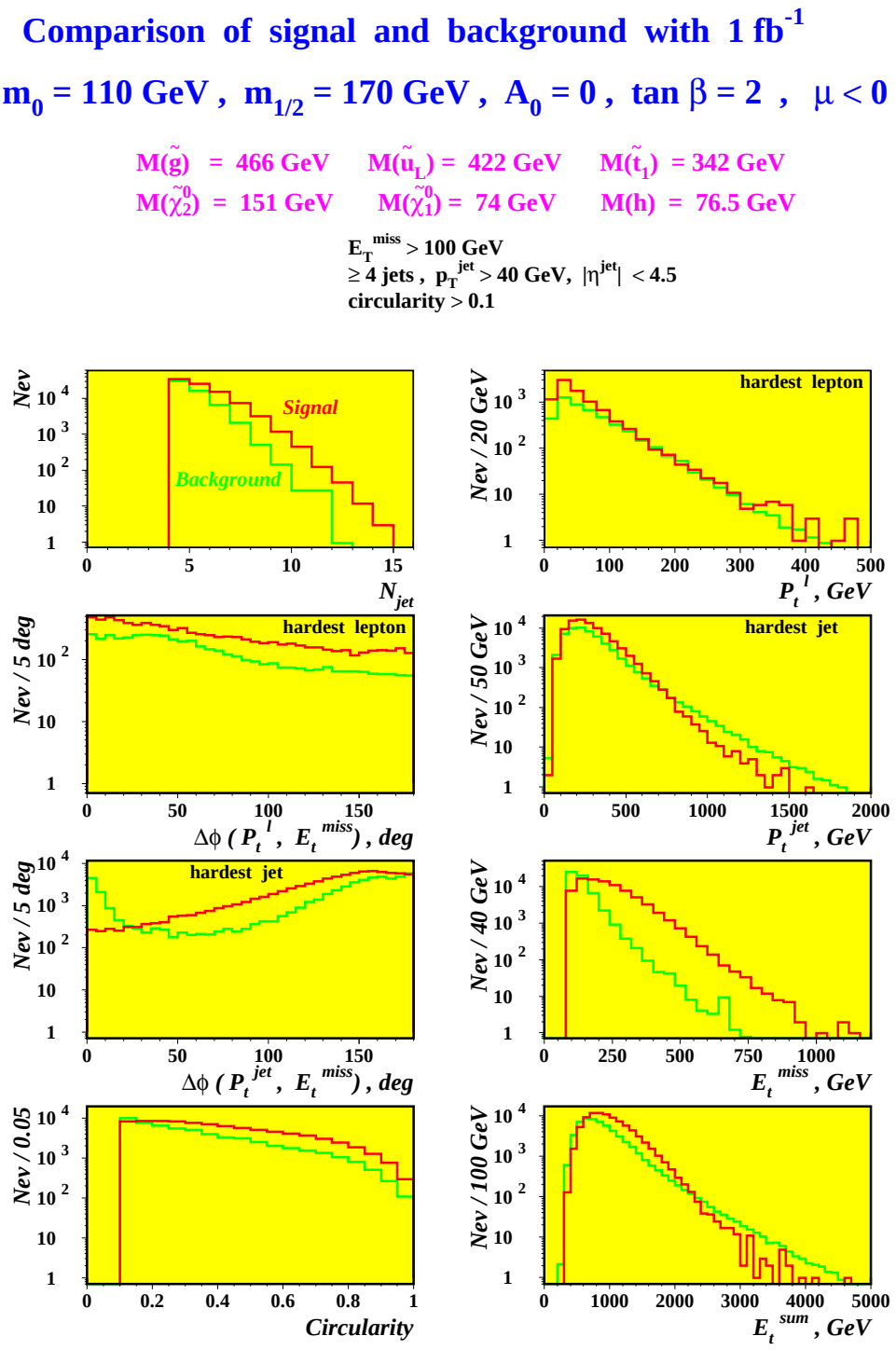

Figure 7: Comparison of mSUGRA signal and SM background distributions at one point accessible already with 1 fb^{-1}.

Comparison of signal and background with 100 fb^{-1}

$m_0 = 500$ GeV , $m_{1/2} = 500$ GeV , $A_0 = 0$, $\tan\beta = 2$, $\mu < 0$

$M(\tilde{g}) = 1224$ GeV $M(\tilde{u}_L) = 1170$ GeV $M(\tilde{t}_1) = 852$ GeV

$M(\tilde{\chi}_2^0) = 427$ GeV $M(\tilde{\chi}_1^0) = 217$ GeV $M(h) = 89.7$ GeV

$E_T^{miss} > 200$ GeV
≥ 4 jets , $p_T^{jet} > 40$ GeV, $|\eta^{jet}| < 4.5$
circularity > 0.1

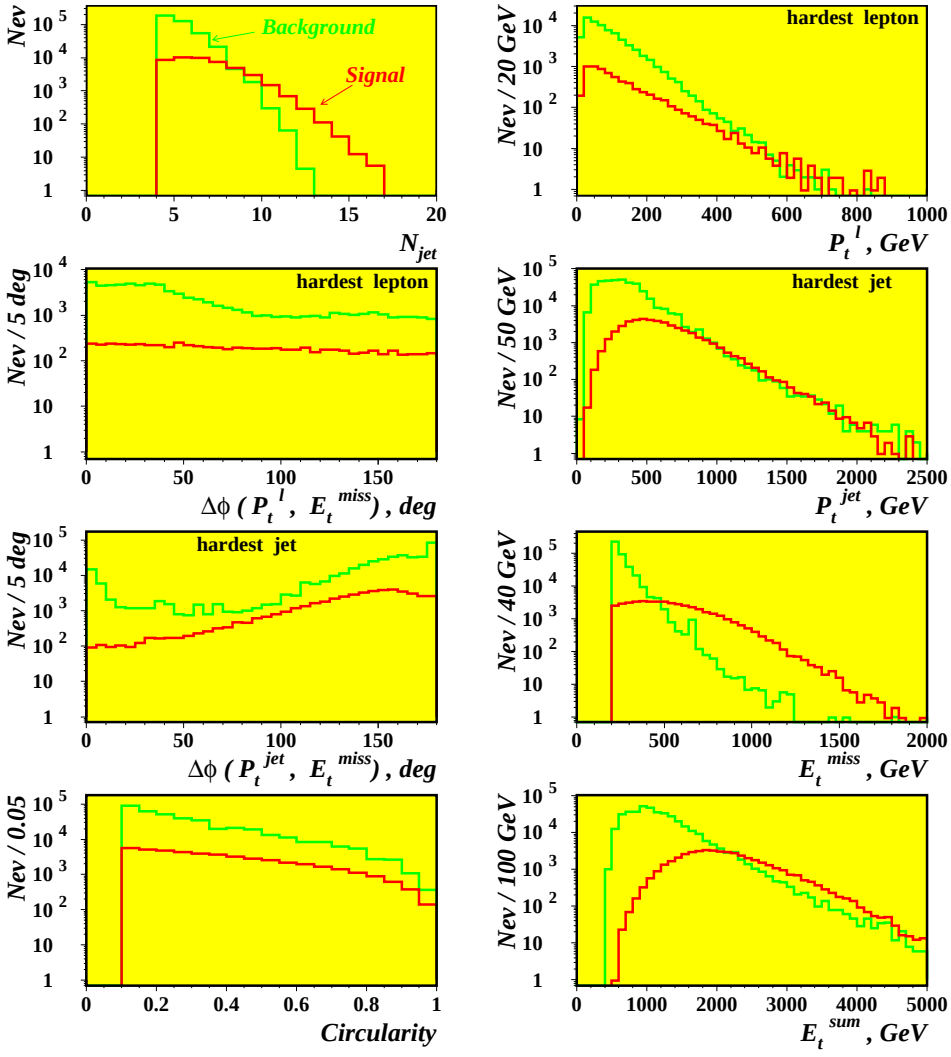

Figure 8: Comparison of mSUGRA signal and SM background distributions at another point requiring $\simeq 100$ fb^{-1} of integrated luminosity.

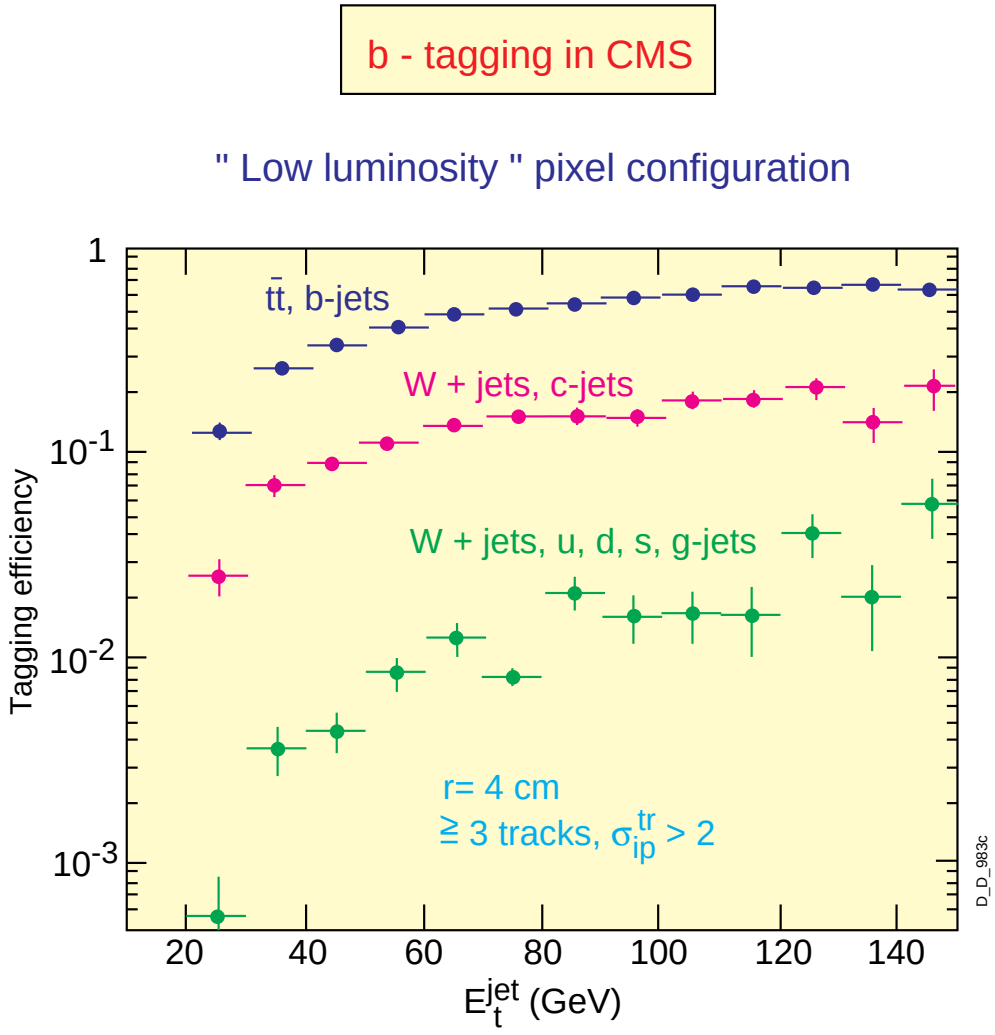

Figure 9: Expected b-tagging performance from impact parameter measurements in CMS tracker with barrel pixel layers at 4 and 7.7 cm radii, with b-tagging algorithm requiring at least 3 tracks of $p_T > 2$ GeV with a transverse impact parameter of $\geq 2\ \sigma$ significance per b-candidate jet.

$h \to b\bar{b}$ *in mSUGRA*

m_0 = 110 GeV, $m_{1/2}$ = 170 GeV, A_0 = 0 , tanβ = 2 , μ < 0

tagging = 100 % , mistagging = 0 %

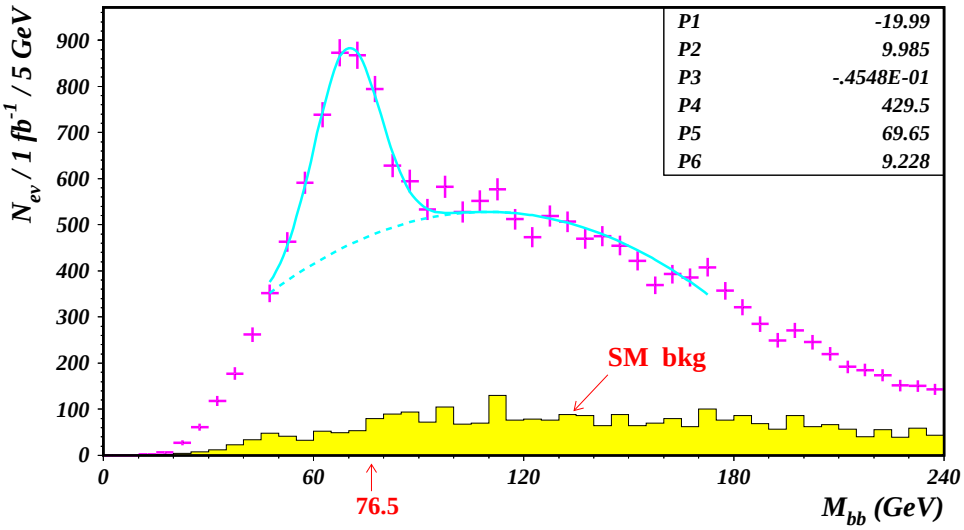

for 55 GeV < M_{bb} < 85 GeV :

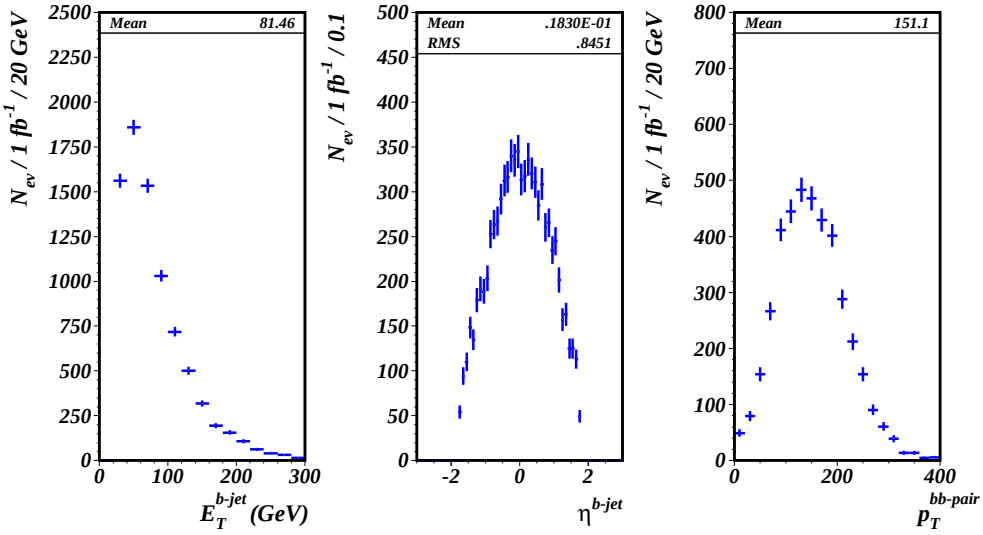

Figure 10: Some distributions for the same parameter space point as in Fig.7 in case of ideal b-tagging performance for 1 fb^{-1}; the lower histograms are for the h mass range 55 < M_{bb} < 85 GeV.

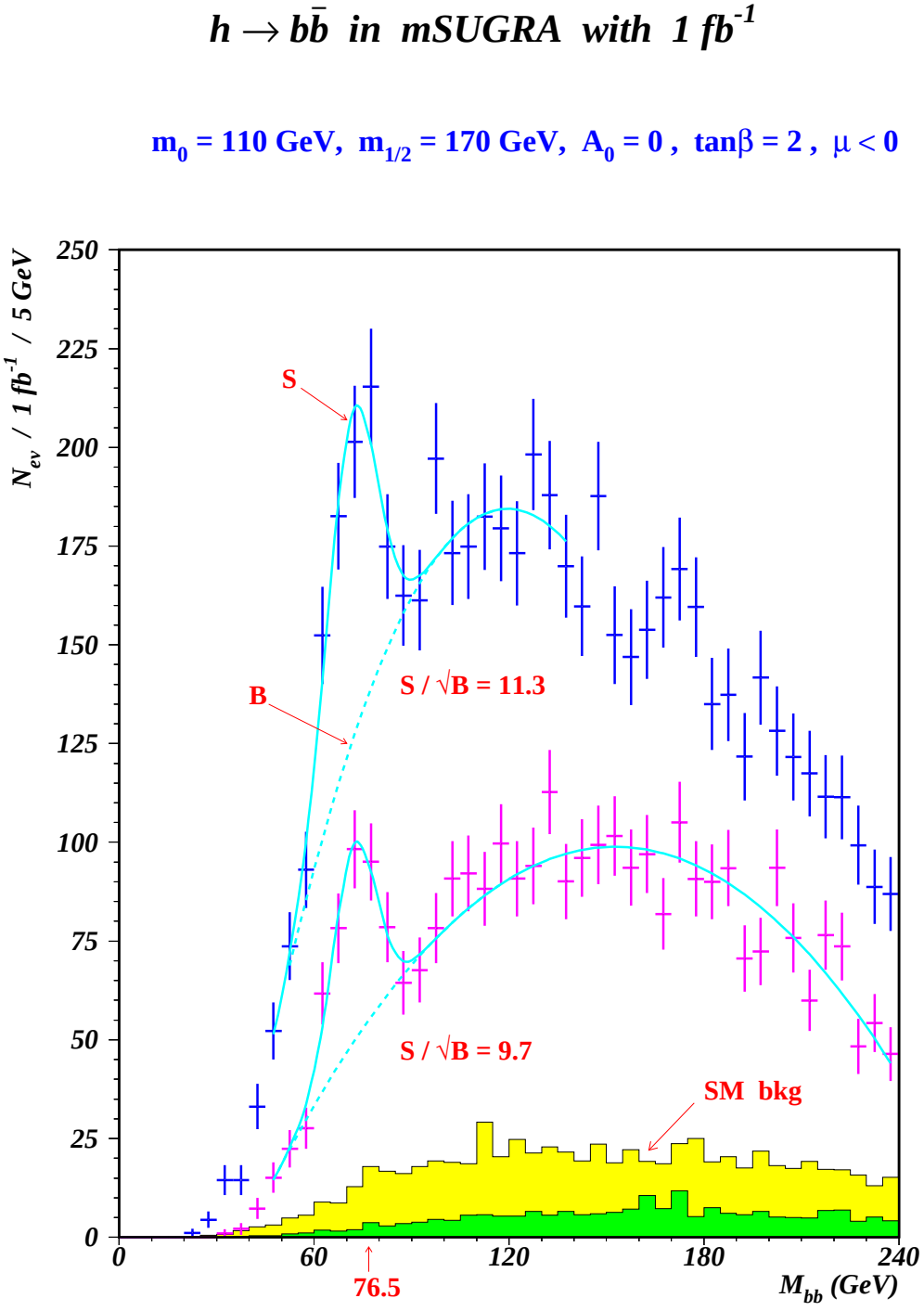

Figure 11: M_{bb} di-jet mass distributions with softer (upper histogram) and harder (lower histogram) cuts, for the same point as in Fig.7 with the expected b-tagging performance of CMS, for 1 fb^{-1}.

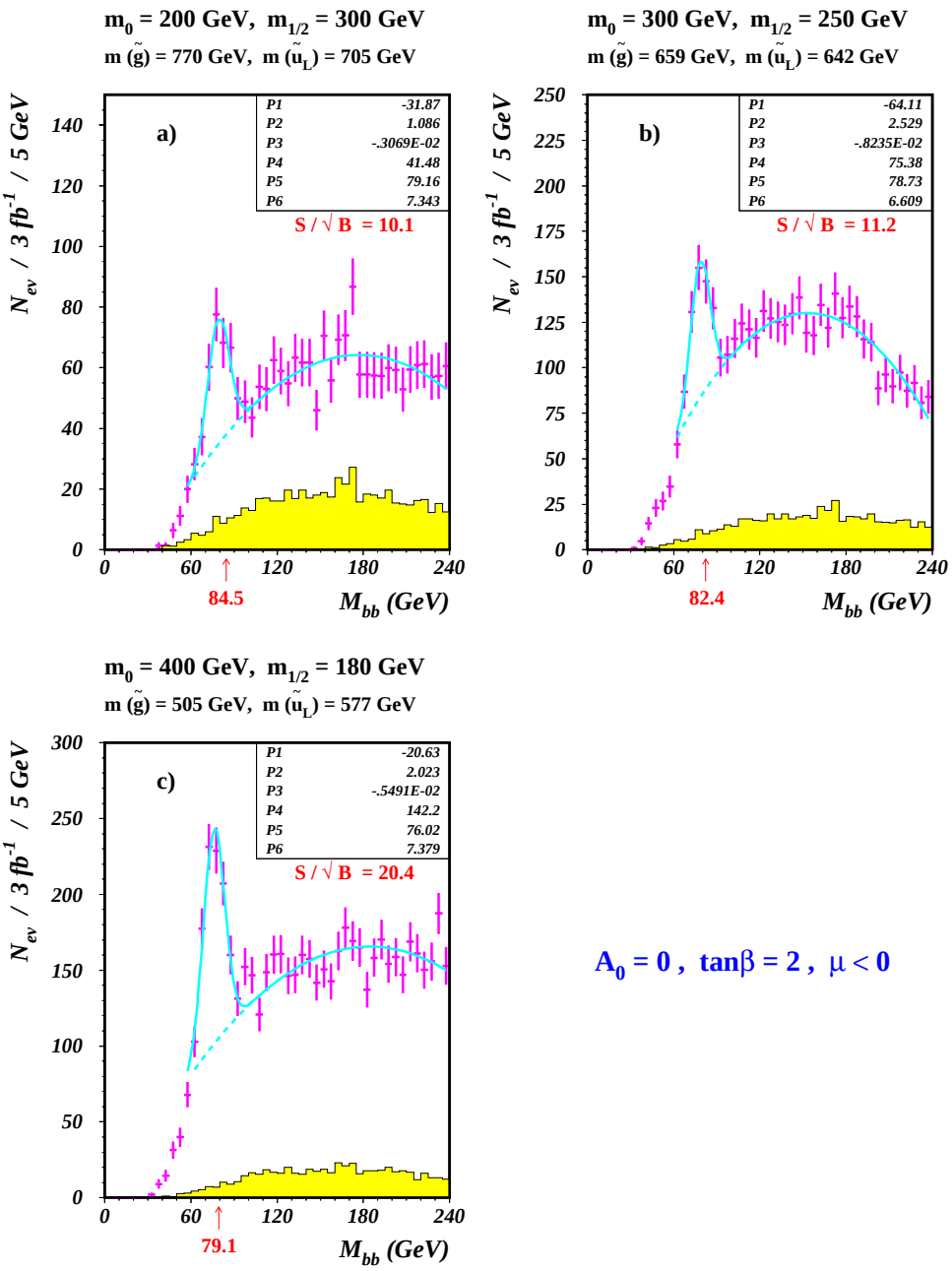

Figure 12: Some points in parameter space accessible already with 3 fb^{-1}. Nominal b-tagging performance of CMS is implemented.

$h \rightarrow b\bar{b}$ *in mSUGRA*

m_0 = 500 GeV, $m_{1/2}$ = 500 GeV, A_0 = 0 , tanβ = 2 , μ < 0

tagging = 100 % , mistagging = 0 %

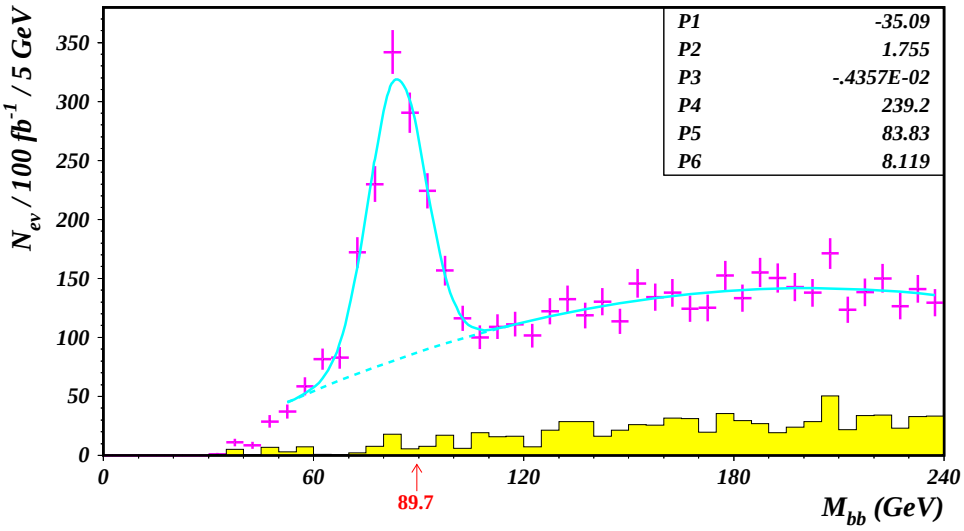

for 70 GeV < M_{bb} < 100 GeV :

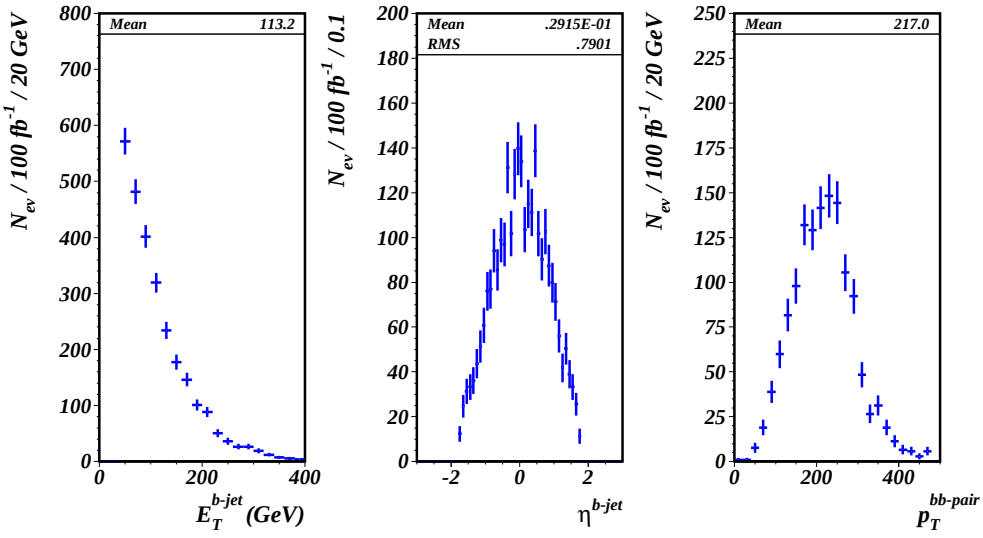

Figure 13: Distribution for the same point in parameter space as in Fig.8 in case of ideal tagging performance.

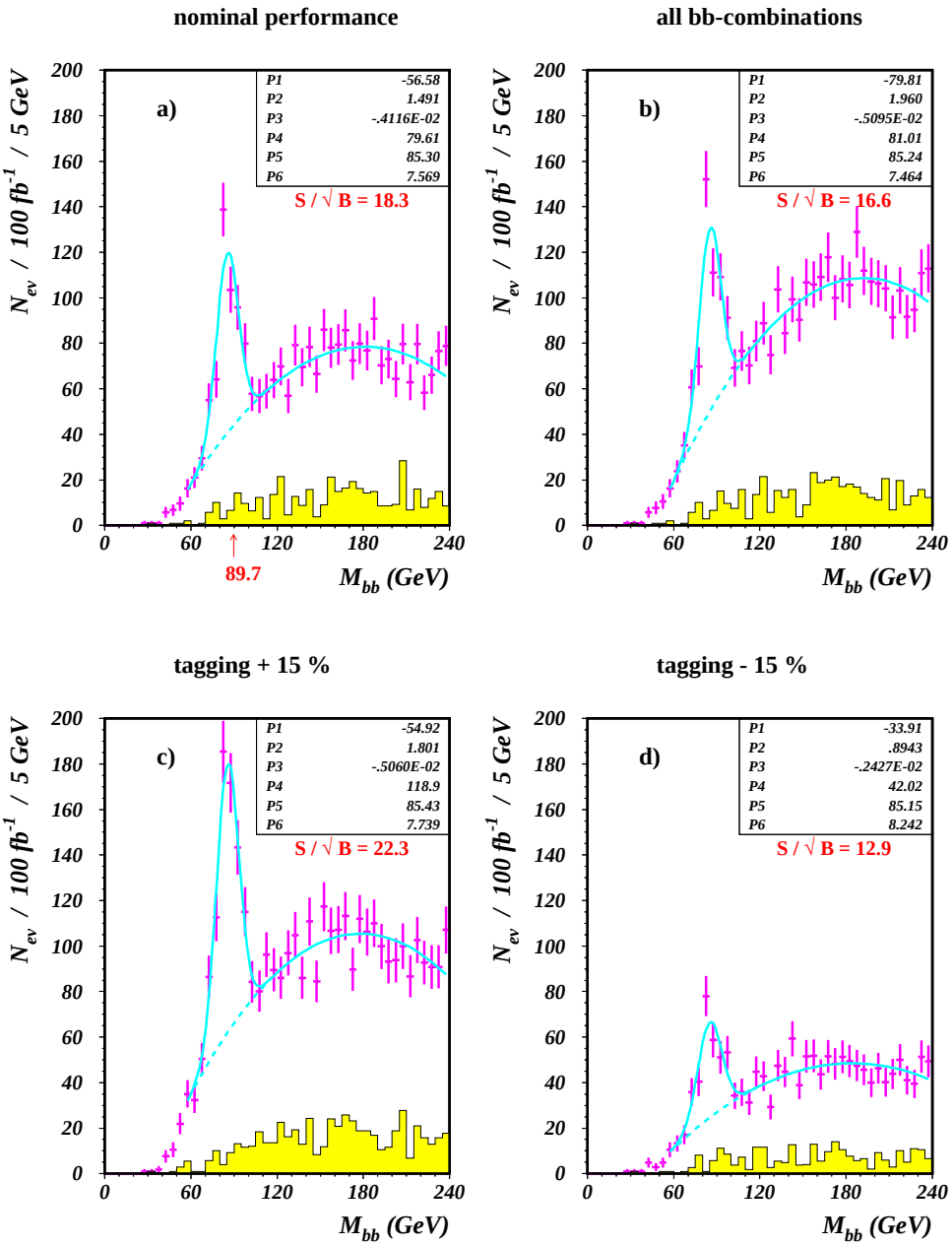

Figure 14: Influence of the various instrumental factors on signal observability in the same parameter space point as in Fig.8 with 100 fb^{-1} : a) with "nominal" b-tagging performance and data selection, b) all bb-combinations per event are included in histogram, c) b-tagging efficiency increased by 15% (absolute shift) and d) b-tagging efficiency decreased by 15% , the mistagging probability is nominal one in all cases.

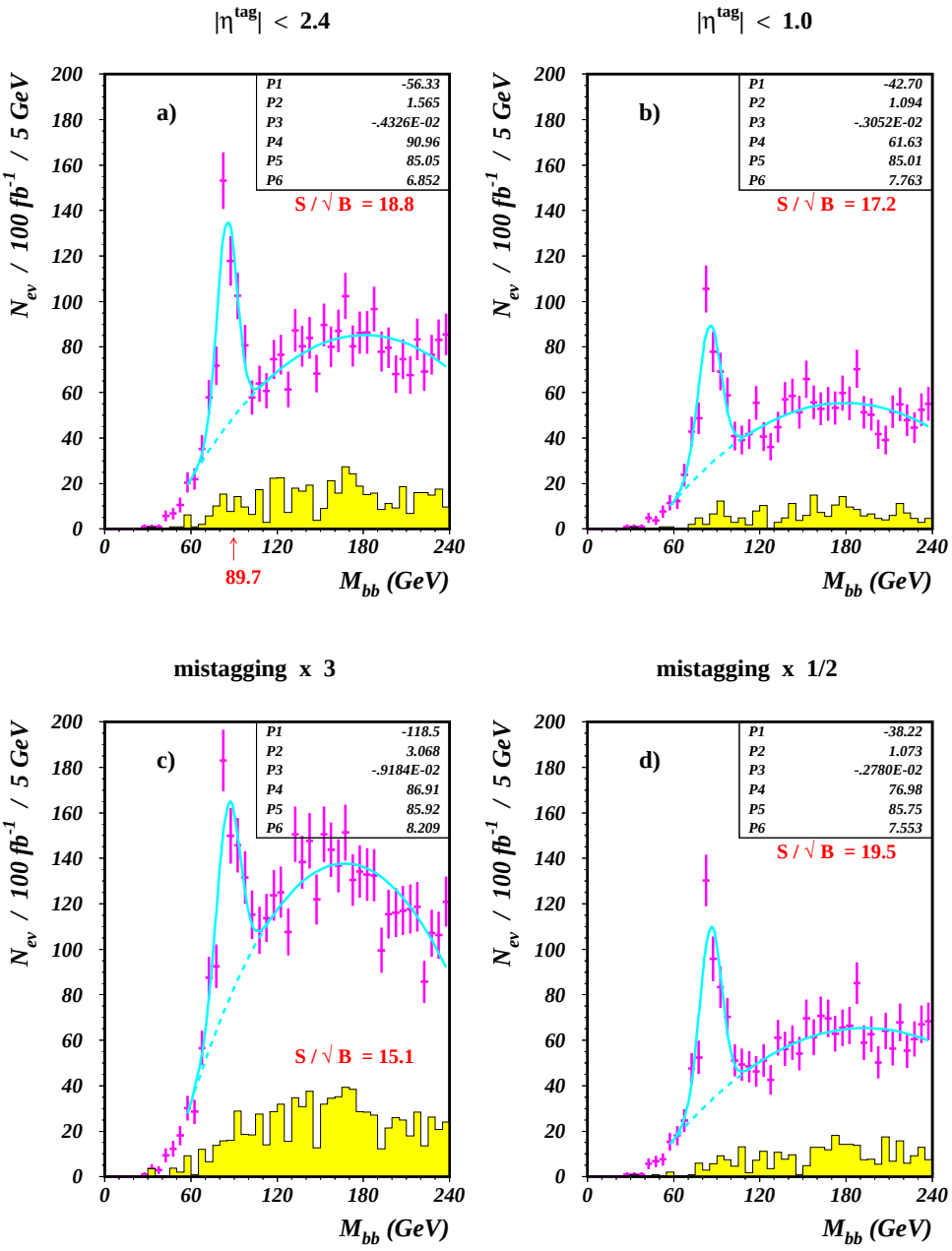

Figure 15: Influence of various instrumental factors on $h \to b\bar{b}$ signal visibility in the same parameter space point as in Fig.14 : a) tagging acceptance increased compared to "nominal" $\mid \eta \mid < 1.75$ up to $\mid \eta \mid = 2.4$, b) tagging acceptance decreased to $\mid \eta \mid = 1.0$, c) mistagging probability increased by a factor of 3 and d) mistagging probability decreased by a factor of 2 relative to nominal expectations.

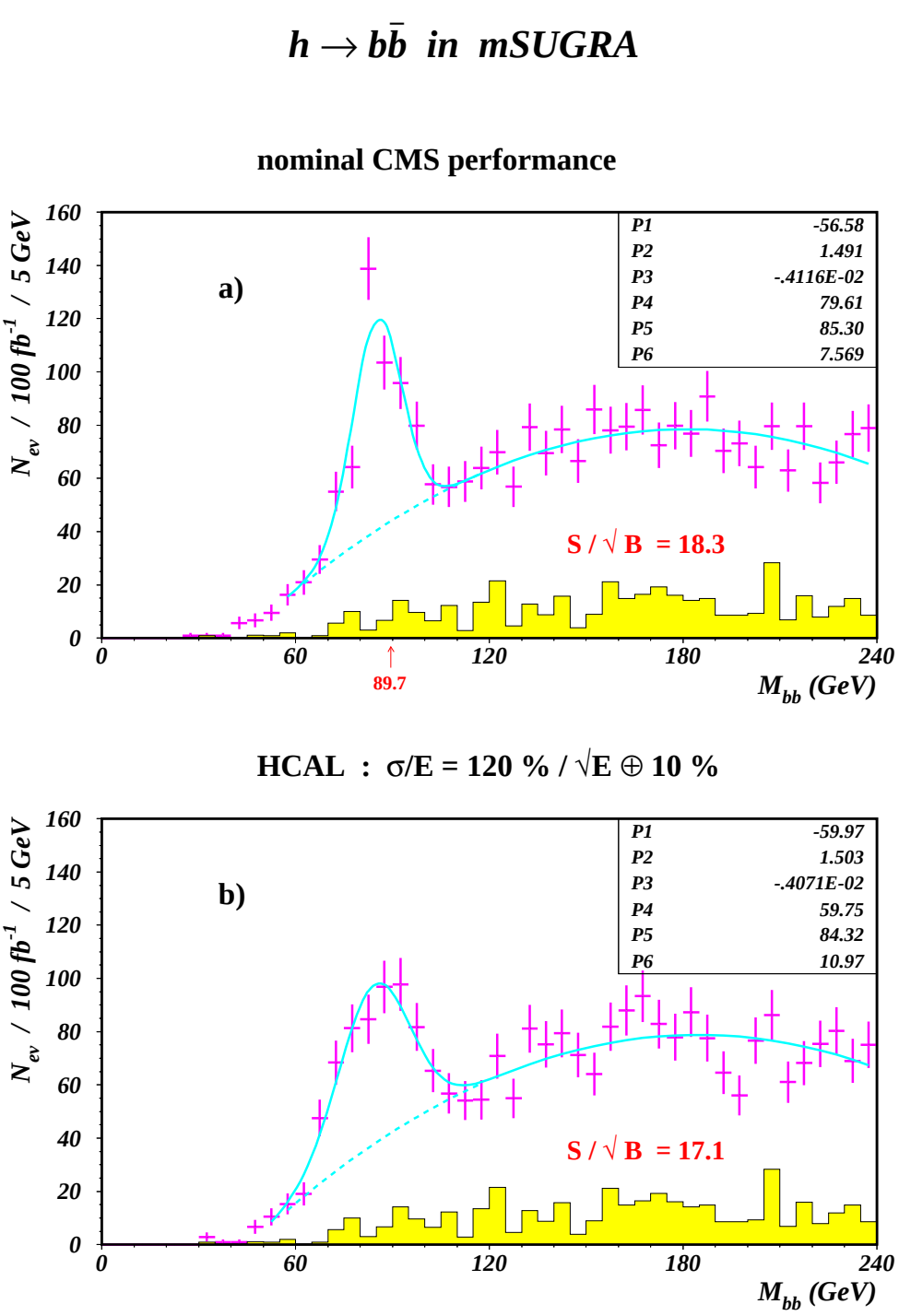

Figure 16: Effect of the assumed single hadron energy resolution on the signal visibility. Same point as in Figs.13, 14 and 15. Note that b-tagging is here performed with impact parameter measurement, not with ”leptons in jets”.

$h \to b\bar{b}$ *in mSUGRA*

m_0 = 600 GeV, $m_{1/2}$ = 600 GeV, A_0 = 0 , tanβ = 2 , μ < 0

$M(\tilde{g})$ = 1454 GeV $M(\tilde{u}_L)$ = 1389 GeV $M(\tilde{t}_1)$ = 1003 GeV
$M(\tilde{\chi}^0_2)$ = 512 GeV $M(\tilde{\chi}^0_1)$ = 262 GeV M(h) = 91.2 GeV

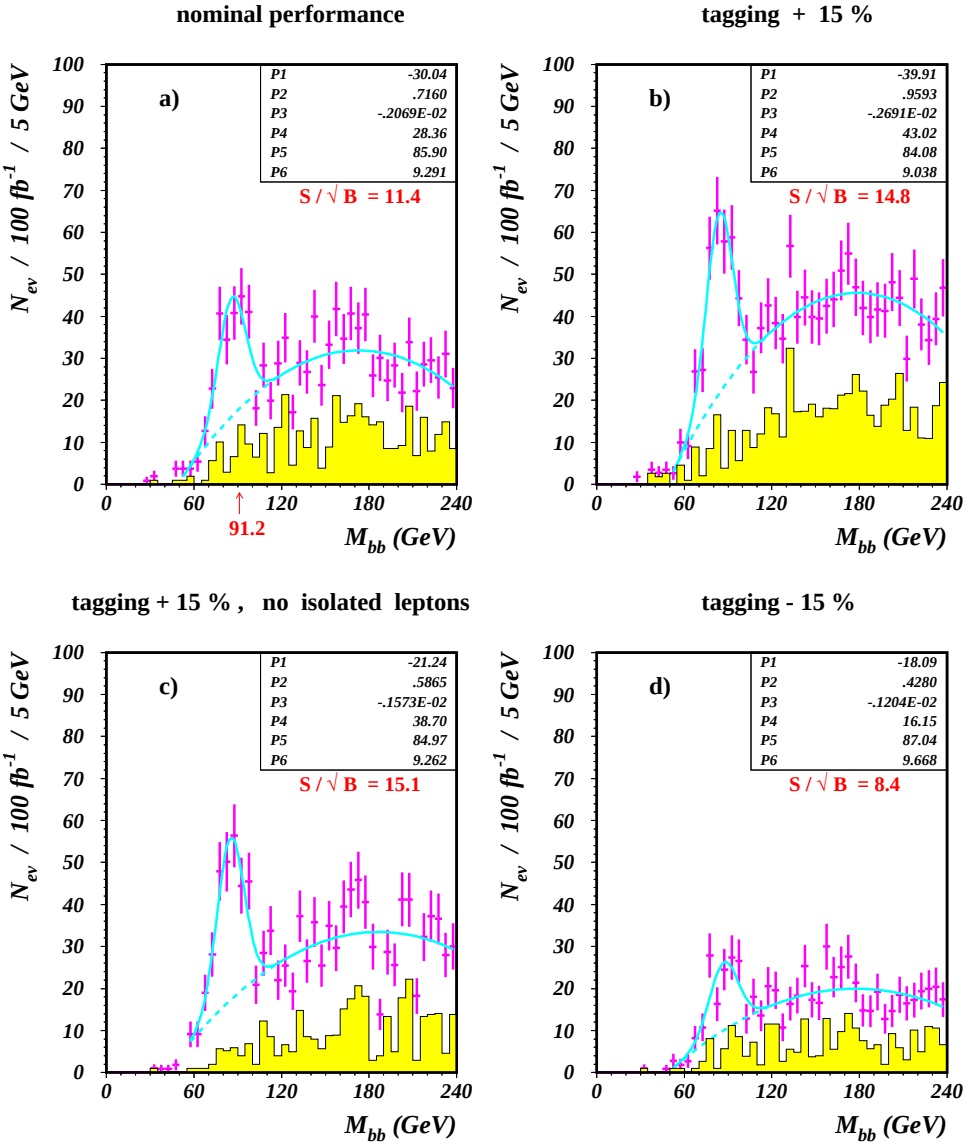

Figure 17: Effect of tagging efficiency on signal visibility at an "extreme" search point : $m_0 = m_{1/2} = 600$ GeV , $A_0 = 0$, $\tan\beta = 2$, $\mu < 0$, near the edge of explorable domain with 100 fb^{-1}.

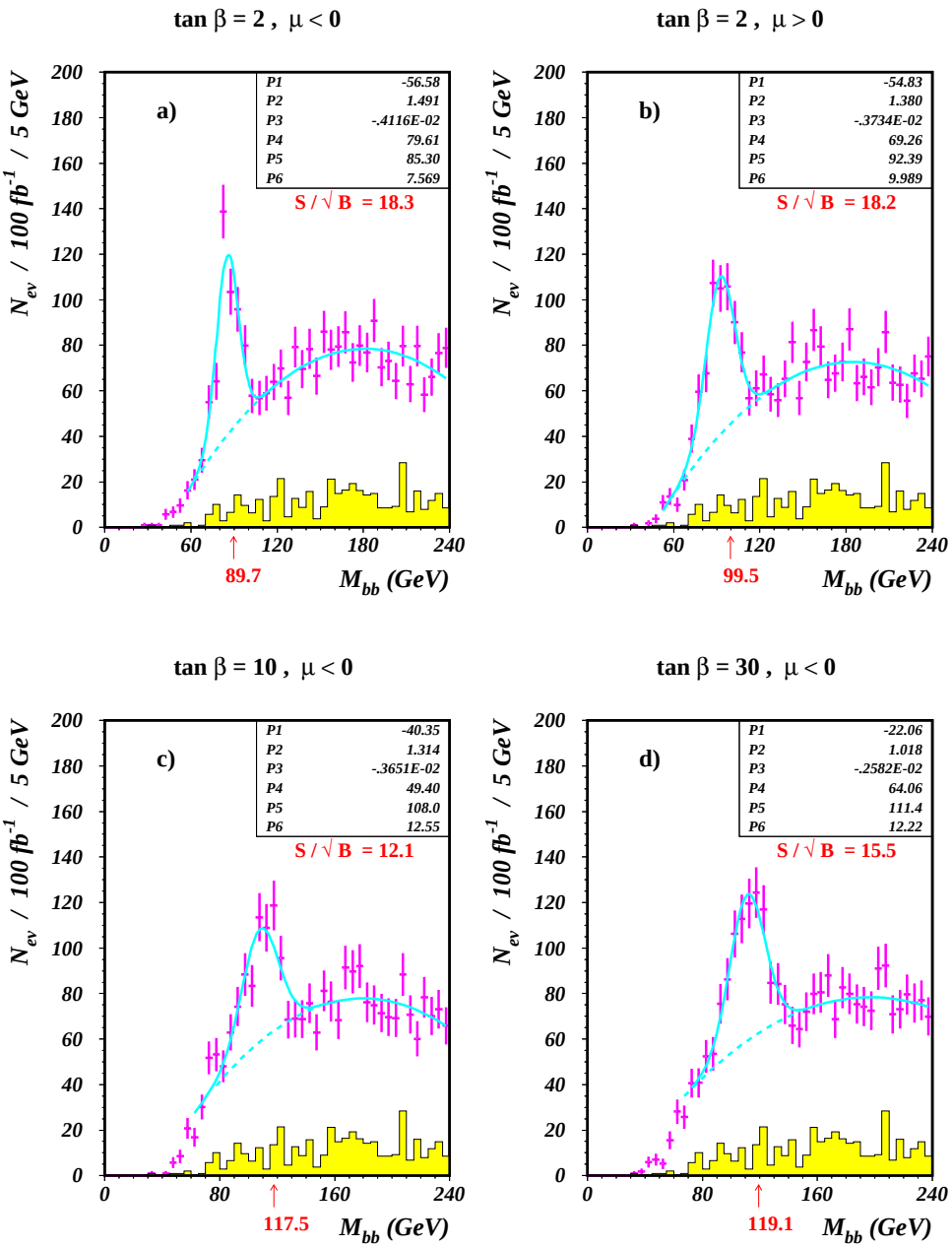

Figure 18: Dependence of the $h \to b\bar{b}$ signal visibility on m_h over the allowed range $\sim$ 80 to 120 GeV, varying tanβ and sign(μ) at a fixed m_0=$m_{1/2}$=500 GeV. Nominal CMS instrumental performance, 100 fb^{-1} integrated luminosity.

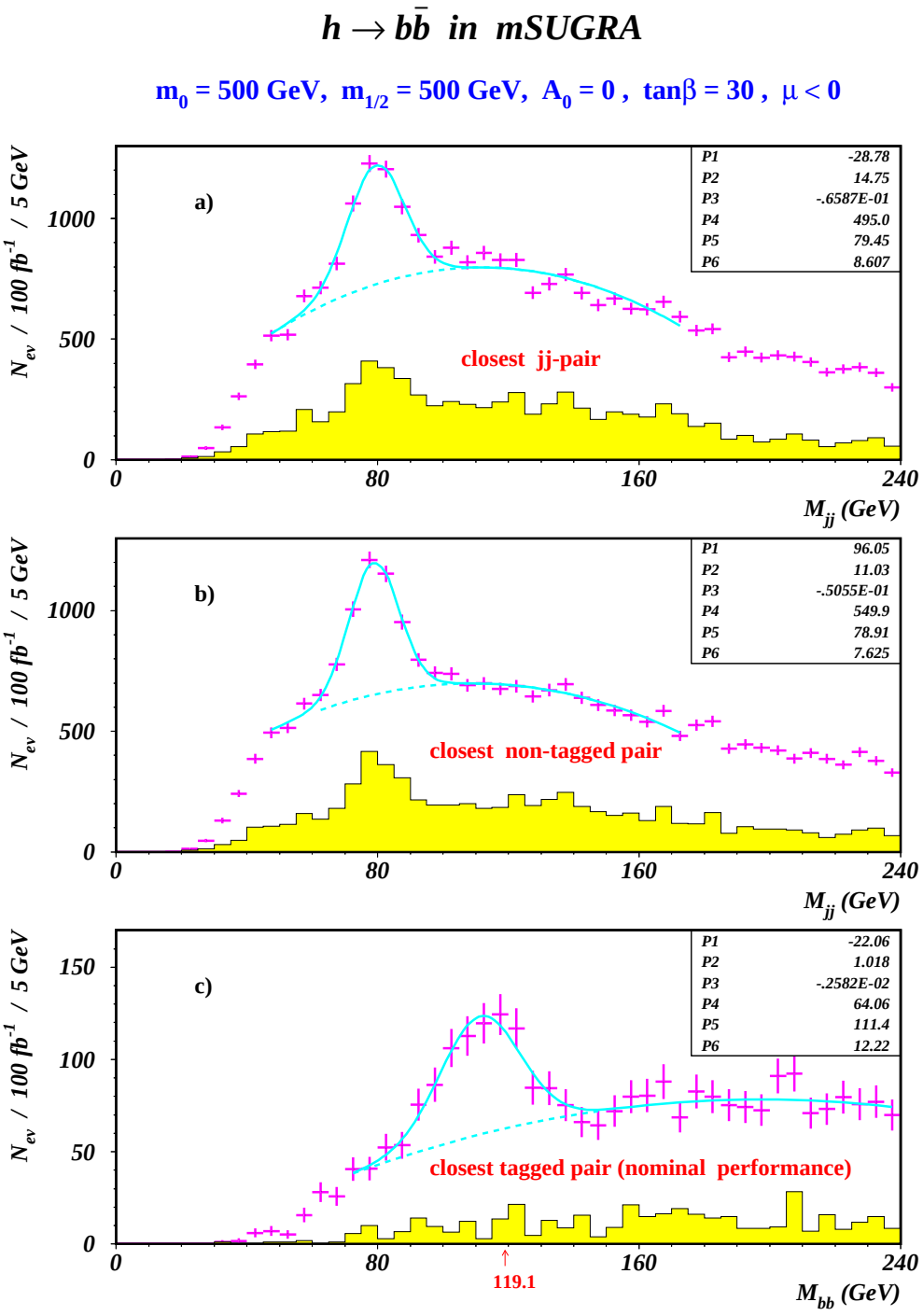

Figure 19: Study of possible confusion (misidentification) between $W \to jj$ and $h \to b\bar{b}$ in some point of parameter space with 100 fb^{-1} : a) jet-jet effective mass if only one closest jj-pair is taken per event regardless b-tagging, the $W \to jj$ peak is clearly visible in both signal and SM background distributions, b) same as previous one, but closest pair is taken among non-tagged jets, c) same as previous ones, but closest pair per event is taken among b-tagged jets, with no visible contribution from $W \to jj$ decays with nominal CMS b-tagging and mistagging performance. Fig 19c is the same as 18d.

$h \to b\bar{b}$ *in mSUGRA*

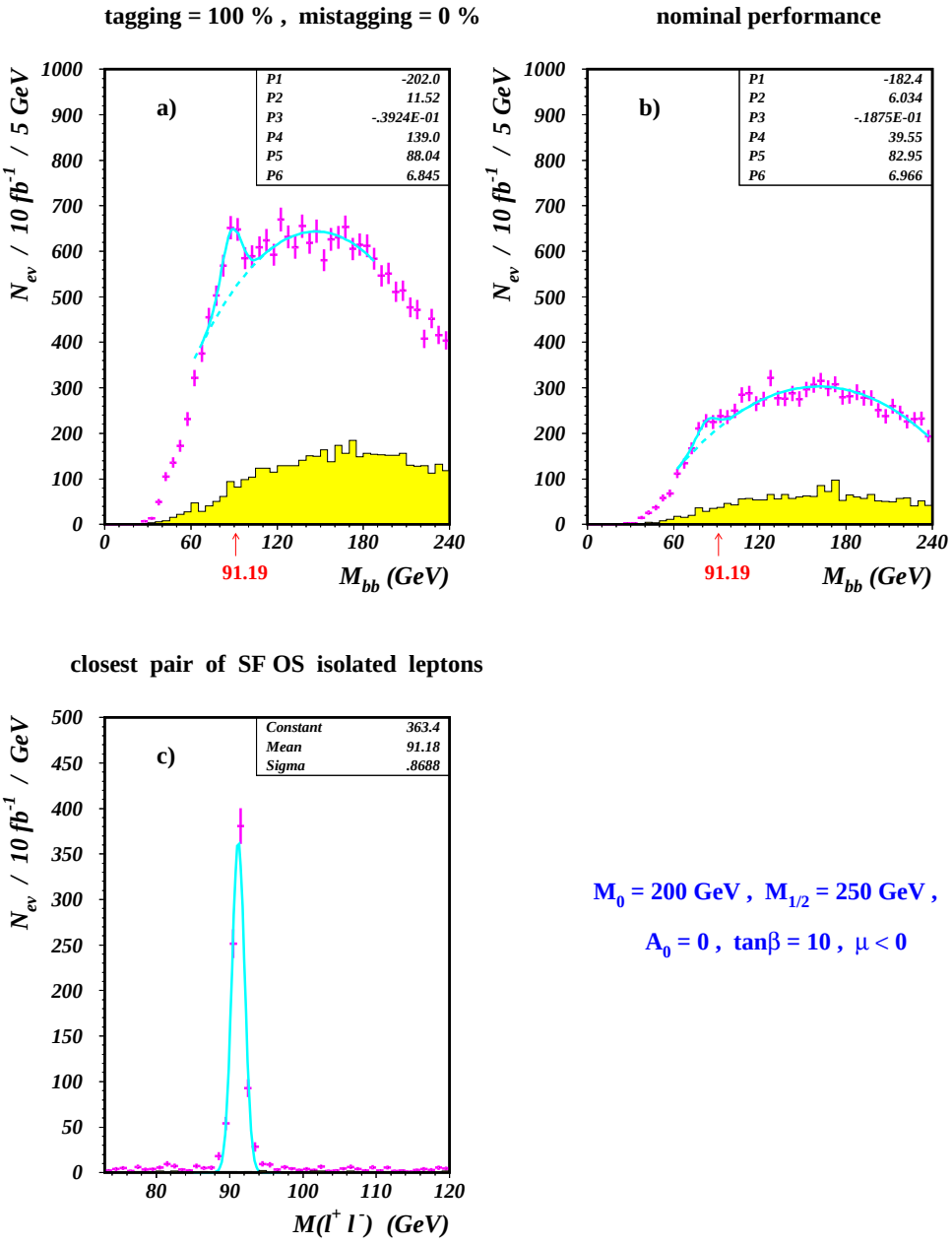

Figure 20: Study of possible confusion between $Z \to b\bar{b}$ ($c\bar{c}$) and $h \to b\bar{b}$ at point m_0 = 200 GeV , $m_{1/2}$ = 250 GeV , A_0 = 0 , tanβ = 10, $\mu < 0$, with 10 fb^{-1}. Despite the presence of a weak M_{bb} peak, only the $\tilde{\chi}_2^0 \to \tilde{\chi}_1^0$ Z channel is open, which can be easily confirmed by Z peak in l^+l^- channel : a) $Z \to b\bar{b}$ with ideal b-tagging performance, b) $Z \to b\bar{b}$ (+$c\bar{c}$) with expected CMS tagging performance, c) $Z \to l^+l^-$ with same statistics and cuts as in previous Figure.

Domains of visibility of the $h \to b\bar{b}$ peak with nominal CMS performance in mSUGRA-SUSY

$S / \sqrt{B} > 5$

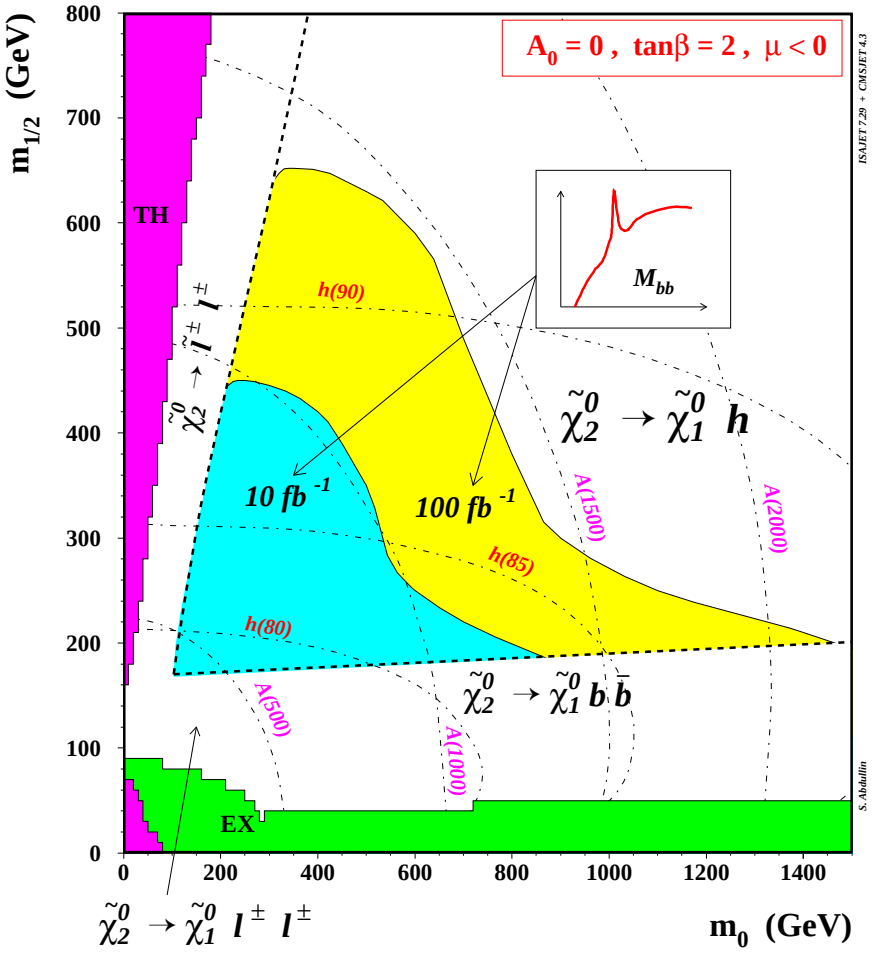

Figure 21: 5 σ visibility contours of $h \to b\bar{b}$ for $A_0 = 0$, $\tan\beta = 2$, and $\mu < 0$ with 10 and 100 fb^{-1}. See also comments in text.

Domains of visibility of the $h \to b\bar{b}$ peak with nominal CMS performance in mSUGRA-SUSY

$S / \sqrt{B} > 5$

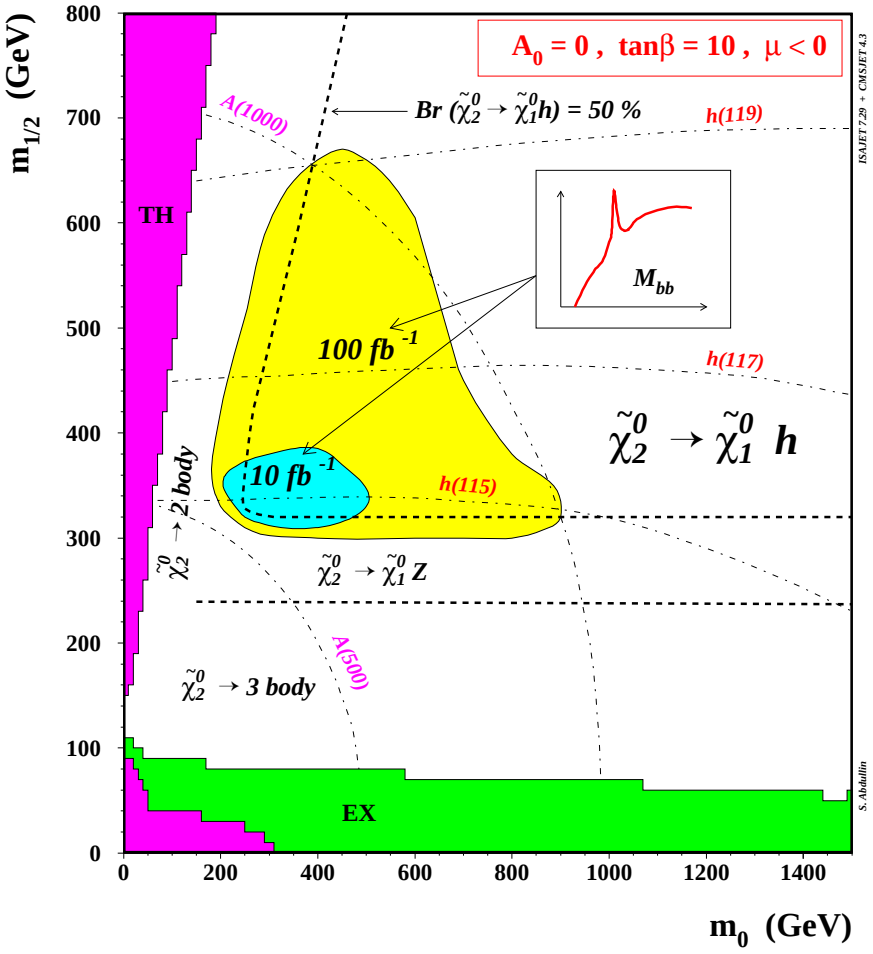

Figure 22: 5 σ visibility contours of $h \to b\bar{b}$ for $A_0 = 0$, $\tan\beta = 10$, and $\mu < 0$ with 10 and 100 fb^{-1}. See also comments in text.

Domains of visibility of the $h \to b\bar{b}$ peak with nominal CMS performance in mSUGRA-SUSY

$S / \sqrt{B} > 5$

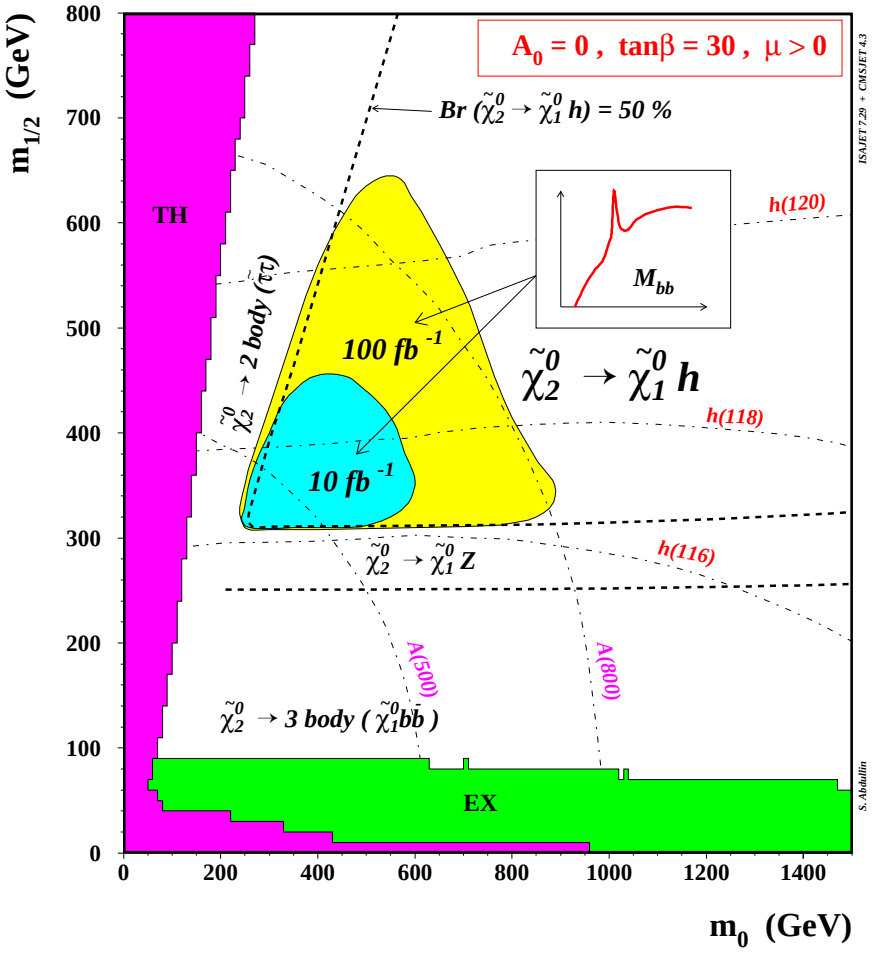

Figure 23: 5 σ visibility contours of $h \to b\bar{b}$ for $A_0 = 0$, $\tan\beta = 30$, and $\mu > 0$ with 10 and 100 fb^{-1}. See also comments in text.